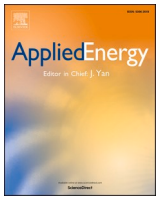
Applied Energy 427 (2027) 128875



Contents lists available at ScienceDirect

Applied Energy

journal homepage: www.elsevier.com/locate/apenergy



Repurposing gas power stations for modular nuclear and hydrogen systems: a techno-economic assessment☆

Ruiyang He, Jianzhong Wu *, Shuai Yao

School of Engineering, Cardiff University, Cardiff CF24 3AA, United Kingdom

HIGHLIGHTS

- Repurposing is formulated through inherited brownfield site constraints.
- Land availability and legacy grid limits shape feasible site pathways.
- Reactor choice is optimised endogenously under repurposing constraints.
- SOEC electricity–heat demand is linked to reactor outlet temperature.
- Nuclear hydrogen integration lowers LCOE by improving plant utilisation under the studied assumptions.

ARTICLE INFO

Keywords:
Repurposing
Advanced nuclear technology
Hydrogen co-generation
High-temperature electrolysis
Techno-economic optimisation

ABSTRACT

In the UK, many fossil-fuel power stations are approaching retirement, yet these sites retain valuable brownfield assets, notably developed industrial land and high-capacity grid connections, and can be repurposed for low-carbon generation. Repurposing such sites for low-carbon generation could therefore offer three linked advantages: lower upfront capital requirements through reuse of grid connections and developed industrial land; shorter project delivery times by reducing permitting needs and avoiding lengthy grid-connection queues; and higher system value through the provision of dispatchable flexibility and improved asset utilisation. This study examines repurposing end-of-life gas power stations into modular nuclear plants and further enabling hydrogen integration via high-temperature electrolysis, where the electricity-heat split is governed by endogenous reactor choice. A repurposing-oriented optimisation framework is proposed to embed inherited brownfield constraints, particularly land availability and grid-export limits, while co-optimising technology selection with hourly unit commitment and economic dispatch. Under the selected representative-week simulations, results show that the repurposed modular nuclear can deliver system-level flexibility comparable to that of gas turbines while meeting brownfield constraints. Nuclear-hydrogen integration further increases reactor utilisation by using co-located electrolysis as a flexible local demand for nuclear-derived electricity and heat, eliminating renewable curtailment and substantially reducing plant-level levelised cost of electricity (LCOE) relative to power-only repurposing under these simulations. Among the electrolyser options, high-temperature electrolysis coupling gives the lowest plant-level levelised cost of hydrogen (LCOH), while producing the largest hydrogen output with the lowest plant-level upfront investment. This advantage arises from the ability of high-temperature electrolysis to use both electricity and cost-effective nuclear heat, reducing reliance on electricity-priced input energy. Sensitivity analysis identifies nuclear and high-temperature electrolyser capital costs as the main upward cost drivers, while stack lifetime remains the key durability-related lever. Overall, the findings indicate that brownfield nuclear-hydrogen integration can provide a valuable pathway for converting retiring thermal power station sites into flexible low-carbon power and hydrogen production assets.

☆ This article is part of a Special issue entitled: 'APEN-Disco HSI 2025(Wu - invite only)' published in Applied Energy.

* Corresponding author.
E-mail address: wuj5@cardiff.ac.uk (J. Wu).

https://doi.org/10.1016/j.apenergy.2026.128875
Received 30 March 2026; Received in revised form 29 July 2026; Accepted 15 September 2026
Available online 2 October 2026
0306-2619/© 2026 The Authors. Published by Elsevier Ltd. This is an open access article under the CC BY license (http://creativecommons.org/licenses/by/4.0/).

Nomenclature

List of abbreviations

ANT	advanced nuclear technology
AMR	advanced modular reactor
CCGT	combined cycle gas turbine
HTSE	high-temperature steam electrolysis
LCOE	levelised cost of energy
LCOH	levelised cost of hydrogen
MILP	mixed-integer linear programming
NHES	nuclear hybrid energy systems
PEM	proton exchange membrane
SMR	small modular reactor
SOEC	solid oxide electrolysis cell

List of symbols

A	site footprint (acre)
a	slope coefficient of linear regression
b	intercept coefficient of linear regression
c	cost coefficient
d	electricity demand (MW)
i	unit
k	type
M	a sufficiently large constant used in Big-M reformulation
m	hydrogen mass produced (kg)
N	number of installed units
p	electrical power (MW)
Q	specific energy requirement (kWh $kg_{H_2}^{-1}$)
q	thermal power (MW)
sdb	standby
T	outlet temperature (°C)
t	time
u	electrolyser unit
x	installation decision variable
y	operating status variable
z	binary variable for limiting regime selection
ϕ	allocation coefficient
el	electrolyser
η	efficiency
π	price

1. Introduction

The UK government's Clean Energy Superpower Mission is framed around two pillars, delivering clean power by 2030 and accelerating to net zero by 2050, which places rapid decarbonisation of the power system at the centre of UK energy policy [1]. Consistent with this trajectory, National Grid ESO's Future Energy Scenarios project a steady decline in unabated gas capacity to 2050 across pathways [2]. While these retirements are necessary for decarbonisation, they also create a strategically important brownfield opportunity: end-of-life gas power station sites retain valuable inherited assets, particularly high-capacity grid connections and developed industrial land, that can materially reduce redevelopment cost and shorten delivery timelines for low-carbon replacement projects. This matters because grid connection works alone typically account for £14.4–17.3 million of project costs for 100–1200 MW sites [3], while reusing existing connections may also avoid multi-year queueing and consenting delays that can extend beyond seven years for greenfield developments [4]. Reuse of established industrial land can further reduce lead times by simplifying site characterisation, planning, and environmental permitting requirements [5]. Repurposing therefore offers not only an asset-reuse opportunity, but also system value by preserving the role of these locations as strategically sited sources of dispatchable low-carbon energy within a decarbonising electricity system.

Among the clean technology options for repurposing retired gas power infrastructure, advanced nuclear technologies (ANTs), used here in the UK sense as an umbrella category encompassing water-cooled small modular reactors (SMRs) and non-water-cooled advanced modular reactors (AMRs), offer a compelling brownfield pathway because their delivery model and plant characteristics align well with constrained, grid-connected industrial sites [6]. Compared with large conventional builds, ANTs are explicitly designed for modular fabrication and repeatable on-site assembly, helping to shorten construction schedules and reduce delivery and financing risk. Operationally, they can provide firm low-carbon capacity while supporting a renewables-dominated system [7,8] through load-following and ramping services [9]; critically, xenon-induced spatial stability generally improves as core size reduces, mitigating a key manoeuvring constraint associated with large light-water reactors [10,11]. They are also land efficient, with the Rolls-Royce SMR (470 MWe) requiring only around 10 acres, compared with 428 acres for Hinkley Point C (3.2 GW). In safety terms, many SMR/ANT concepts emphasise passive and simplified safety functions (e.g., reliance on natural circulation and other inherent mechanisms), which can ease siting and emergency-planning burdens relative to traditional large units [12]. Importantly, the UK is already moving in this direction: on 10 June 2025 the government announced Rolls-Royce SMR as the preferred bidder for the UK SMR programme, with initial plans for three units, and subsequent communications have indicated Wylfa as the intended host location for three Rolls-Royce SMRs [13].

Building on these repurposing advantages, a key question is how ANTs can be operated to maximise both system value and asset utilisation, particularly under increasing challenges from variable renewables [14]. In contrast to combined cycle gas turbines (CCGTs), where variable operating costs scale primarily with fuel burn, nuclear plants are characterised by low marginal costs but high upfront capital costs, making sustained utilisation and revenue recovery particularly important. When electricity-side demand or price signals would otherwise drive nuclear output down, diverting available generation to electrolysis provides a practical flexibility outlet, converting low-carbon energy into a storable product rather than leaving capacity underused [15,16]. Among electrolysis options, low-temperature proton exchange membrane (PEM) and alkaline (ALK) technologies draw almost entirely on electricity [17], whereas high-temperature steam electrolysis (HTSE) using solid oxide electrolysis cell (SOEC) can utilise both electrical and thermal inputs [18]. Because input energy constitutes a major share of the LCOH, supplying part of the process energy as heat, particularly at higher temperatures, can reduce the required electrical input for steam generation and heating, thereby improving overall conversion efficiency and hydrogen economics; this makes SOEC coupling a natural complement to ANT-based co-generation pathways [19].

Recent studies on nuclear-enabled hydrogen production are largely situated in nuclear hybrid energy systems (NHES) research, where electrolysis is modelled as a flexible demand that converts surplus low-carbon output into hydrogen. System-level studies typically pair renewables with a pre-specified reactor design and optimise system sizing and operation against techno-economic and reliability metrics, showing that HTSE integration can improve overall utilisation and reduce renewable curtailment under explicit operating constraints [20]. Other studies place greater emphasis on operational realism by treating HTSE as a controllable load and demonstrating its feasibility under dynamic operating limits and grid-support requirements, including through multi-timescale scheduling in renewable-intensive systems and with

associated reductions in renewable curtailment [21,22]. In parallel, market-oriented studies evaluate nuclear-hydrogen co-generation as a revenue-stabilisation pathway, using dispatch optimisation across electricity and hydrogen markets and framing hydrogen production as an alternative to inefficient nuclear load-following [23,24]. Process-integration studies, often using flowsheet-based modelling, quantify levelised costs for SMR-supplied HTSE and wider multi-product configurations (e.g., direct air carbon capture coupling), while noting that results are sensitive to local system conditions and assumptions [25,26]. Complementary SOEC-focused analyses provide component-level economic and uncertainty insights (e.g., the value of waste-heat integration and dominant cost drivers), and methodological contributions introduce uncertainty quantification and surrogate models to accelerate design–operation evaluation [27–31], alongside tool-based assessments of nuclear–renewable hybrids with hydrogen storage using representative months and stochastic wind energy data [32]. Despite this progress, the existing literature does not fully address the requirements of deployment-oriented brownfield repurposing. Most studies are effectively framed as greenfield design problems and therefore do not represent the inherited site constraints that can determine feasible deployment at retired power stations, particularly available land and legacy grid-export capacity. In addition, the nuclear technology is usually specified in advance rather than selected within the optimisation, which means that differences across candidate ANTs are not resolved endogenously. Third, reactor-specific outlet temperature is rarely propagated into high-temperature electrolysis performance within an integrated optimisation framework, meaning that the electricity-heat split in hydrogen production is typically not determined consistently with reactor choice.

Building on these gaps, this study addresses a question that existing studies on nuclear-hydrogen integration have not resolved: what is the least-cost feasible repurposing pathway for gas power stations using modular nuclear and hydrogen co-generation? A mixed-integer linear programming framework is therefore developed that, to our knowledge, is the first to bring three features together in a single repurposing-oriented model: (i) inherited brownfield constraints, particularly land availability and electricity export capacity; (ii) endogenous reactor choice through joint optimisation of advanced nuclear technology selection and installed capacity; and (iii) explicit thermal coupling between technology-specific outlet temperature and the electricity-heat split in high-temperature steam electrolysis. This allows hydrogen production, plant operation, and system economics to be evaluated consistently within a site-constrained brownfield setting.

The remainder of the paper is organised as follows. Section 2 presents the overall system description and problem statement, and details the mathematical formulations for the ANT and electrolysis technologies together with the optimisation objectives, binding constraints, solution approach, and sensitivity-analysis set-up. Section 3 summarises the techno-economic parameters and key assumptions adopted, including ANT and electrolyser cost and performance inputs, as well as the representative-week construction and the electricity and hydrogen price settings. Section 4 introduces the Peterhead case study and reports the optimisation results for two repurposing pathways, namely ANT-only operation and ANT-hydrogen co-generation, alongside comparative discussion and sensitivity results. Section 5 concludes with the principal findings and implications for UK brownfield deployment.

2. Methodology

2.1. System description and problem statement

A general repurposing problem is considered for end-of-life gas power station sites that retain inherited brownfield assets, particularly existing grid connection capacity and industrial land, and are to be redeveloped as low-carbon nuclear-renewable integrated energy systems. Within this general framework, two representative configurations are defined, as illustrated in Fig. 1. Fig. 1(a) represents a power-only repurposing configuration in which ANTs replace the retiring CCGT plants while continuing to operate alongside wind and PV within NHES, thereby retaining the general role of dispatchable generation in complementing variable renewable output. Fig. 1(b) extends this configuration by integrating electrolysis-based hydrogen production, so that the repurposed plant provides both electricity and hydrogen. In both configurations, the repurposed plant exchanges electricity with the wider power system through the inherited grid connection, while the feasible repurposing design space is restricted by site-specific brownfield constraints, most notably available industrial land and legacy grid-export capacity. The optimisation framework therefore co-determines technology selection, module deployment, and hourly unit operation subject to these inherited constraints.

Hydrogen co-generation is represented through alternative electrolysis pathways. Low-temperature electrolysis options (alkaline and PEM) are modelled as electricity-only conversion routes, while HTSE is represented by SOEC, which requires a co-supply of electricity and thermal energy. The electricity–heat split for SOEC is not imposed as a fixed ratio; instead, it is constrained by the quality of available heat and is therefore linked to the selected ANT technology through its outlet temperature [18]. Hydrogen produced by electrolysis is buffered by on-site storage (treated as part of the balance of plant) before being delivered to a downstream hydrogen market.

The modelling framework is formulated as an integrated planning-and-scheduling co-optimisation, in which structural configuration choices and hourly operational feasibility are determined consistently. Planning decisions select the ANT technology option(s) and installed module counts under inherited repurposing constraints; when hydrogen co-generation is enabled, the planning layer is extended to also select the installed electrolyser capacity, while the electrolyser technology is treated as an exogenous option for comparative assessment. Conditional on these planning outcomes, the scheduling layer optimises hourly unit commitment and economic dispatch of ANT modules and electrolyser operation, including loading levels and the allocation of energy between grid supply and hydrogen production. When HTSE is enabled, the scheduling decisions additionally determine the hourly allocation of reactor thermal output between the power block and electrolysis, creating an explicit trade-off between heat routed to hydrogen production and residual heat available for electricity generation. For clarity, the power-only configuration in Fig. 1(a) is referred to as Scenario 1, and the hydrogen-integrated configuration in Fig. 1(b) as Scenario 2.

2.2. Mathematical models

2.2.1. ANT unit and power-block model

ANTs are modelled as low-carbon, dispatchable units that provide firm capacity and operational flexibility alongside wind and photovoltaic generation. Each unit is represented as a controllable thermal source coupled to a steam-cycle power block, which converts reactor thermal output into turbine electrical output. The thermal-to-electric conversion is captured using a technology-specific efficiency parameter, η_k, indexed by ANT type k. Over the operating range considered, η_k is treated as constant for each ANT type and is not varied with loading level. Unit feasibility is instead enforced through explicit operational constraints introduced in Section 2.3.

In the power-only configuration (Fig. 1(a)), all reactor thermal output is routed to the power block, and turbine electrical output for unit i of type k at time t is given by:

$$p^{tb}_{kit} = \eta_k q^{tb}_{kit} \tag{1a}$$

When hydrogen co-generation is enabled (Fig. 1b), the reactor remains the primary thermal source. If high-temperature electrolysis is deployed, a portion of the available thermal output may be diverted to electrolysis, and the per-unit heat allocation is enforced via:

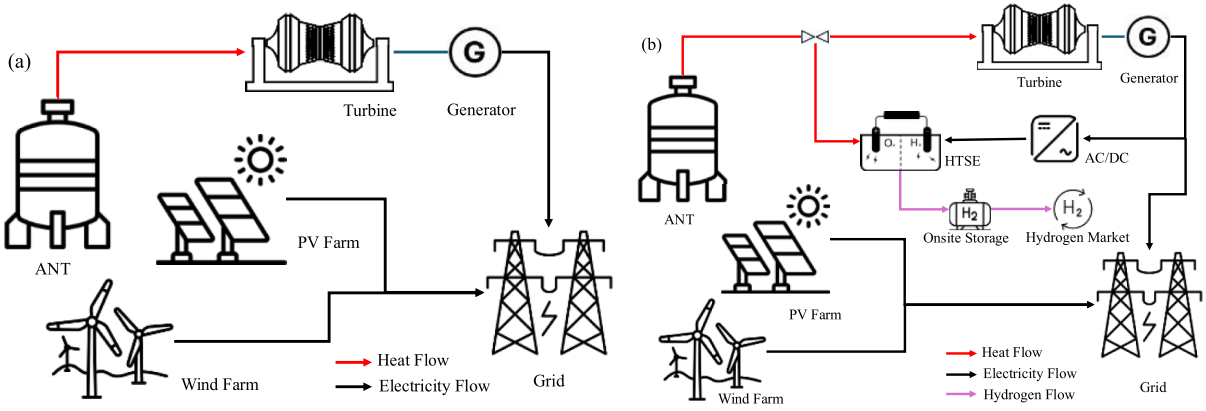


Fig. 1. Alternative configurations of the repurposed nuclear–renewable system at a retired CCGT site: (a) without hydrogen co-generation; (b) with hydrogen co-generation.

$$q^{tb}_{k\,i\,t} = q_{k\,i\,t} - q^{el}_{k\,i\,t} \tag{1b}$$

Turbine electrical output continues to be determined by η_k applied to the thermal input delivered to the power block. For low-temperature electrolysis options, electrolysis is modelled as a flexible electrical load without an explicit thermal co-input; accordingly, $q^{el}_{kit} = 0$ and the power-block relation in (1a) applies.

2.2.2. High temperature electrolysis model

The SOEC model is activated only in the hydrogen-integrated configuration; in the power-only configuration, SOEC-related variables and constraints are inactive. As illustrated in Fig. 2, the SOEC electricity–heat split is inherently temperature-dependent based on data compiled from the National Nuclear Laboratory [18] and the Dalton Nuclear Institute [19]. With increasing available heat temperature, a larger share of the specific energy requirement for hydrogen production can be supplied as thermal input, which correspondingly reduces the required electrical input. Over the temperature range shown, the total specific energy requirement varies only modestly; however, the substitution is systematic and monotonic, with thermal demand increasing and electrical demand decreasing. This behaviour is particularly relevant when high-grade heat is available, as it enables part of the electrical requirement for steam generation and heating to be displaced by thermal energy.

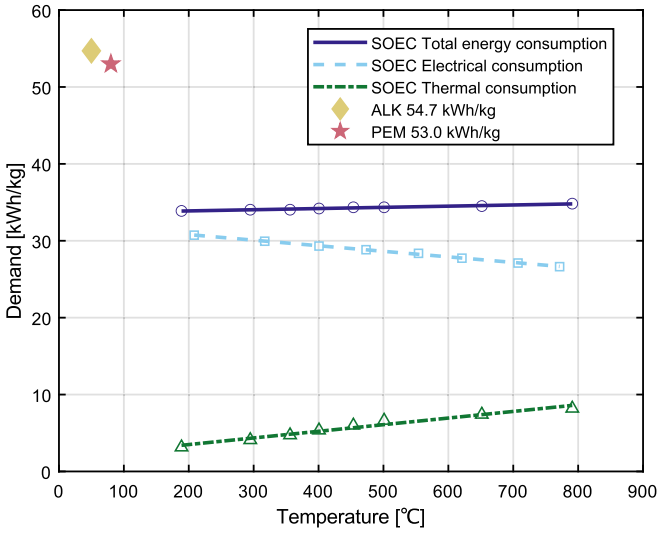


Fig. 2. Temperature-dependent electricity and heat requirements for SOEC hydrogen production [18].

To reflect this mechanism, SOEC performance is represented over a temperature range rather than approximated by a single fixed design point, as is commonly assumed in existing studies. This treatment is necessary because ANTs exhibit materially different outlet temperatures, and these differences translate directly into different SOEC electricity–heat splits. Accordingly, the SOEC electricity and heat coefficients are parameterised as functions of reactor heat grade, so that the implied electrolysis efficiency and operating cost are determined consistently with the selected ANT option and its operating regime, rather than being imposed as a technology-invariant heat requirement. This representation is intended to capture the first-order effect of reactor heat grade on SOEC energy splitting, based on literature-derived relationships [18]. A conservative SOEC thermal-loss allowance [33] is included for each online unit, combining approximately 2–3% heat-transfer loss with an additional approximately 2% auxiliary heating/steam-side requirement.

Building on the temperature-dependent electricity–heat split in Fig. 2, the SOEC model is parameterised as an explicit function of the reactor outlet temperature. For ANT technology k, the outlet temperature T_k determines the SOEC specific energy intensities through linear regressions fitted to Fig. 2:

$$Q_{\mathrm{tot}}(T_k) = a_{tot}T_k + b_{tot}, Q_e(T_k) = a_eT_k + b_e \tag{2}$$

where Q_{tot} and Q_e denote the total and electrical specific energy consumption of SOEC of hydrogen production per kilogram.

The fitted coefficients used are:

$$a_{tot} = 0.001543, b_{tot} = 33.574 \tag{3a}$$

$$a_e = -0.007241, b_e = 32.251 \tag{3b}$$

The thermal specific energy requirement is obtained residually:

$$Q_{\mathrm{th}}(T_k) = Q_{\mathrm{tot}}(T_k) - Q_e(T_k) \tag{4}$$

To express the temperature effect on a combined nominal-capacity basis, two SOEC allocation coefficients are defined:

$$\phi^{\mathrm{soec}}_e(T_k) = \frac{Q_e(T_k)}{Q_{\mathrm{tot}}(T_k)}, \phi^{\mathrm{soec}}_{th}(T_k) = \frac{Q_{\mathrm{th}}(T_k)}{Q_{\mathrm{tot}}(T_k)} = 1 - \phi^{\mathrm{soec}}_e(T_k) \tag{5}$$

Accordingly, the rated input capacity of one SOEC unit on a combined electricity–heat basis, $\overline{P}^{\mathrm{soec}}$, is partitioned into technology-specific upper bounds on its electrical and thermal interfaces:

$$\overline{P}^{\mathrm{soec}}_k = \phi^{\mathrm{soec}}_e(T_k)\overline{P}^{\mathrm{soec}}, \quad \overline{Q}^{\mathrm{soec}}_k = \phi^{\mathrm{soec}}_{\mathrm{th}}(T_k)\overline{P}^{\mathrm{soec}} \tag{6}$$

where $P_{r,k}^{\mathrm{soec}}$ and $Q_{r,k}^{\mathrm{soec}}$ represent the maximum electrical and thermal inputs that can be supplied to the SOEC under ANT technology k. This ensures that the SOEC electricity–heat split is not imposed as a fixed assumption, but is implied by the usable heat grade associated with T_k.

At time t, SOEC energy use is represented by the run-mode electrical input P_{kut}^{soec}, run-mode thermal input Q_{kut}^{soec}, and standby electrical consumption $P_{kut}^{soec,sdb}$. A binary operating indicator $y_{kut}^{soec} \in \{0,1\}$ is used together with an installation indicator $x_u^{soec} \in \{0,1\}$, selected in the planning layer. Standby electrical consumption is incurred when an installed SOEC unit is kept energised in hot-standby mode but is not producing hydrogen in run mode. Following [34], it is modelled as:

$$P_{kut}^{\mathrm{soec,sdb}} = \left(x_u^{\mathrm{soec}} - y_{kut}^{\mathrm{soec}}\right) K_{\mathrm{sdb}}^{\mathrm{soec}} \overline{P}_k^{\mathrm{soec}} \tag{7a}$$

$$y_{kut}^{soec} \le x_u^{soec}, \quad \forall k,u,t \tag{7b}$$

where K_{sdb}^{soec} is the standby electricity coefficient. The total electrical demand of the SOEC unit is therefore $P_{kut}^{soec} + P_{kut}^{soec,sdb}$, whereas Q_{kut}^{soec} is treated separately as the thermal input during operation. The operating status is linked to the installation decision through (7b).

To translate SOEC energy inputs into hydrogen output, the hydrogen-production rate is limited by the co-supply requirement of high-temperature electrolysis. For each technology k, the reactor outlet temperature T_k determines the SOEC-specific energy intensities: an electricity requirement $e_k(T_k)$(MWh$_e$/kg) and a thermal requirement $h_k(T_k)$(MWh$_{th}$/kg). At each time step t, the run-mode electricity and heat supplied to each SOEC unit u are represented by P_{kut}^{soec} and Q_{kut}^{soec}, respectively. The feasible hydrogen-production rate m_{kut} is then determined by the more restrictive of the two energy inputs, which can be expressed using a nonlinear minimum operator.

$$m_{kut} = \min\left(\frac{P_{kut}^{soec}}{e_k}, \frac{Q_{kut}^{soec}}{h_k}\right) \tag{8}$$

To retain MILP tractability, Eq. (8) is linearised with a Big-M reformulation and an auxiliary binary variable $z_{k\,u\,t} \in \{0,1\}$ indicating the limiting regime (electricity-limited versus heat-limited). The following constraints enforce the minimum operator:

$$\begin{cases} \dfrac{Q_{k\,u\,t}^{soec}}{h_k} \le \dfrac{P_{k\,u\,t}^{soec}}{e_k} + M\,(1 - z_{k\,u\,t}) \\ \dfrac{P_{k\,u\,t}^{soec}}{e_k} \le \dfrac{Q_{k\,u\,t}^{soec}}{h_k} + M\,z_{k\,u\,t} \end{cases} \tag{9}$$

deterioration, the SOEC electrical specific energy requirement is increased linearly with cumulative represented hours at an adopted degradation rate of 0.59% per 1000 h [35].

2.2.3. Low temperature electrolysis model

Low-temperature electrolysis (LTE) is represented as an electricity-only conversion process with no thermal co-input. LTE is therefore modelled as a flexible electrical demand that can be scheduled to draw a portion of turbine electrical output, creating an explicit trade-off between grid export and hydrogen production.

Hydrogen production from LTE is captured using a linear electricity-to-hydrogen conversion. Let p_{ut}^{lte} denote the electrical power consumed by the LTE unit $u$at time t(MW), and $\Delta t$the dispatch interval (h). The hydrogen mass produced over the interval, m_{ut}^{lte}(kg), is given by:

$$m_{ut}^{lte} = \frac{p_{ut}^{lte}\,\Delta t}{e_l^{lte}} \forall u,t \tag{11}$$

where e_l^{lte} is the technology-specific electricity requirement (specific electricity consumption) for LTE (MWh/kg $-$ H_2); Differences between ALK and PEM are represented through parameterisation of e_r^{lte}(and associated techno-economic inputs), while the present subsection focuses on the conversion relationship.

2.3. Optimisation models

2.3.1. Optimisation objectives

A unit commitment and economic dispatch (UC/ED) formulation is adopted to identify the least-cost feasible repurposing outcome over the selected horizon. The optimisation is expressed as a net-revenue maximisation problem, in which electricity and hydrogen revenues are valued against annualised investment costs and operating costs. Plant-level LCOE and LCOH are reported as post-processed performance indicators based on the optimised schedules and annualised costs.

2.3.1.1. Scenario 1: power-only repurposing. In the power-only configuration, revenues arise only from electricity exported to the grid. The objective maximises electricity sales revenue minus operating costs and annualised fixed charges, while allowing slack variables to be penalised when required to maintain feasibility. The resulting objective is written as:

$$max\left[\pi\sum_t p_t^{ANT,grid} - \sum_t\sum_k\sum_i p_{kit}^{tb}\left(c_k^{VOM} + c_k^{fuel}\right) - \sum_t\sum_k\sum_i c_k^{SU} v_{kit}^{ant} - \sum_k\sum_i P_k\left(c_k^{FOM} + CRF_k \bullet OCC_k\right) - \lambda_{ens}\sum_t p_t^{ens} - \lambda_{curt}\sum_t p_t^{curt}\right] \tag{12}$$

$$\begin{cases} m_{k\,u\,t} \le \dfrac{P_{k\,u\,t}^{soec}}{e_k} \\ m_{k\,u\,t} \le \dfrac{Q_{k\,u\,t}^{soec}}{h_k} \\ m_{k\,u\,t} \ge \dfrac{P_{k\,u\,t}^{soec}}{e_k} - M\,z_{k\,u\,t} \\ m_{k\,u\,t} \ge \dfrac{Q_{k\,u\,t}^{soec}}{h_k} - M\,(1 - z_{k\,u\,t}) \end{cases}, m_{k\,u\,t} \ge 0, z_{k\,u\,t} \in \{0,1\} \tag{10}$$

where M is a sufficiently large constant that deactivates the non-binding lower bound in each regime. This formulation ensures that $m_{k\,u\,t}$ is bounded by both energy inputs and is forced to coincide with the active limiting term, while preserving linearity. To capture the performance

where π is the electricity price, k is the type of ANT technology and i is the corresponding number of a specific ANT type. $p_t^{ANT,grid}$ represents the electricity sold to power system while p_{kit}^{tb} denotes the electrical power output of each specific ANT. P_k is the rated electrical capacity. The parameters c_k^{VOM}, c_k^{FOM}, c_k^{fuel}, c_k^{SU} are the variable O&M cost, fixed O&M cost, fuel cost, and start-up cost for the technology k, respectively. OCC_k represents the overnight capital cost (OCC) of ANT type k and CRF_k is the corresponding capital recovery factor to annualise the investment cost. p_t^{ens} and p_t^{curt} are the associated unmet electricity and renewable curtailment with penalty coefficients $\lambda_{ens}$and λ_{curt}.

The capital recovery factor (CRF) is defined as:

$$CRF = \frac{r(1+r)^n}{((1+r)^n - 1)} \tag{13}$$

where r is the discount rate and n is the asset lifetime. A discount rate of $r = 5\%$ is used, with technology-specific lifetimes applied to each asset class.

2.3.1.2. Scenario 2: hydrogen co-generation enabled. When hydrogen co-generation is enabled, net revenue is maximised by jointly valuing electricity exports and hydrogen production, while accounting for costs incurred by both the ANT fleet and the electrolysis subsystem. HTSE via SOEC is represented with coupled electricity and thermal co-inputs; for LTE options (ALK and PEM), electrolysis is electricity-only and the thermal term is identically zero.

The objective is written as:

$$max\left[\pi\sum_t p_t^{ANT,grid} + \pi_{H_2}\sum_t\sum_u m_{ut} - \sum_t\sum_k\sum_i\left(p_{kit}^{tb} + \frac{P_k}{Q_k}q_{kit}^{el}\right)\left(c_k^{VOM} + c_k^{fuel}\right) - \sum_k\sum_i P_k\left(c_k^{FOM} + CRF_k \bullet OCC_k\right) - \sum_r\sum_u P_l^{el}\left(c_r^{el,OPEX} + CRF_l^{el} \bullet OCC_l^{el}\right) - \lambda_{ens}\sum_t p_t^{ens} - \lambda_{curt}\sum_t p_t^{curt}\right] \quad (14)$$

where π_{H_2} is the hydrogen price and m_{ut} is the hydrogen output of electrolyser unit u. As in Scenario 1, $p_t^{ANT,grid}$ denotes the ANT-derived electricity supplied to the grid. The term q_{kit}^{el} denotes reactor thermal output allocated to electrolysis, while P_k/Q_k converts this thermal allocation into an electricity-equivalent quantity for ANT operating-cost accounting. In Scenario 2, installed ANT units are assumed to remain online throughout the dispatch horizon; therefore, no time-dependent ANT start-up cost is included. The superscript "el" denotes the electrolyser subsystem. For LTE options (ALK and PEM), q_{kit}^{el}=0, whereas SOEC uses both electrical and thermal inputs. Grid demand is treated as the primary obligation because $p_t^{ens}$is assigned a sufficiently large penalty, ensuring that hydrogen production is not increased at the expense of grid supply.

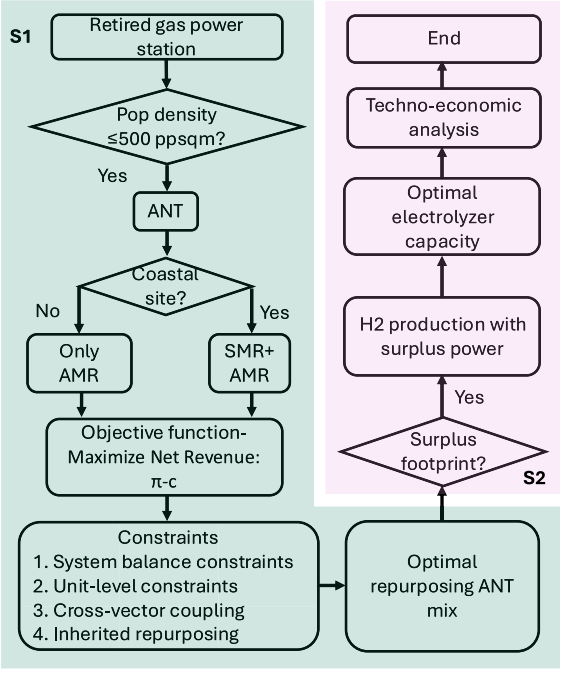


Fig. 3. Workflow for siting screening, repurposing optimisation, and techno-economic evaluation of retired gas power station sites.

2.3.2. System constraints

Fig. 3 summarises the workflow adopted in this study. Candidate retired gas power station sites are first screened against siting criteria, after which the repurposing optimisation is solved subject to inherited site limits, and the resulting techno-economic outcomes are evaluated. Consistent with this workflow, the optimisation model is formulated with four classes of constraints: (i) system balance constraints, (ii) unit-level operational feasibility constraints, (iii) cross-vector coupling constraints (active only when hydrogen co-generation is enabled), and (iv) inherited repurposing constraints reflecting legacy site limits. Constraint classes (i), (ii) and (iv) apply in both configurations, with class (ii) applied to the set of controllable assets represented (ANT units in the power-only configuration, and both ANT units and electrolysers when co-generation is enabled). Class (iii) is required only in the hydrogen co-generation configuration to capture electricity–heat–hydrogen coupling, including reactor heat allocation for SOEC; LTE options remain electricity-only demands without an explicit thermal co-input.

(i) **System balance constraints**

The system is operated to serve the exogenous grid electricity demand at every dispatch interval. In Scenario 1, the optimisation schedules available generation (wind, PV, and dispatchable ANT output) to meet the grid load, with any excess represented as curtailment. In Scenario 2, grid demand remains the primary obligation, and any surplus electricity beyond d_t may be allocated to on-site hydrogen production (via electrolysis), thereby trading off against renewable curtailment but never displacing load supply. Because the repurposed plant interacts with the wider grid through an inherited connection interface, the power exchanged with the grid is additionally bounded by the legacy connection capacity introduced in Section (iv).

Accordingly, the allocation of electrical power is represented through separate ANT-side and grid-side balances. First, the turbine electrical output of the ANT fleet is allocated between electricity supplied to the grid and electricity consumed by the co-located electrolyser:

$$\sum_k\sum_i p_{kit}^{tb} = p_t^{ANT,grid} + \sum_{u\in\mathscr{U}^{el}} p_{ut}^{el}, \forall t \quad (15a)$$

where $p_t^{ANT,grid}$ denotes the ANT-derived electricity supplied to the grid and p_{ut}^{el} denotes the electrical input to electrolyser unit u. For LTE, $p_{ut}^{el} = p_{ut}^{lte}$. For SOEC, p_{ut}^{el} includes both run-mode and standby electrical consumption, i.e., $p_{ut}^{el} = \sum_k\left(P_{kut}^{soec} + P_{kut}^{soec,sdb}\right)$. Thus, the electrolyser is supplied by co-located ANT-derived electricity rather than external wind or PV generation.

Second, the total electricity supplied through the grid-facing pathway is given by:

$$p_t^{sys} = p_t^{w} + p_t^{pv} + p_t^{ANT,grid}, \forall t \quad (15b)$$

where p_t^{sys} is the total electricity supplied to the wider power system, and p_t^{w} and p_t^{pv} are the utilised wind and PV outputs, respectively.

Grid demand is then satisfied subject to an electricity-not-served slack variable:

$$p_t^{sys} + p_t^{ens} = d_t, p_t^{ens} \geq 0, \forall t \quad (16)$$

where d_t denotes the exogenous grid electricity demand.

Renewable curtailment is represented separately as the difference between the available and utilised wind and PV outputs:

$$p_t^{w} + p_t^{w,curt} = \bar{p}_t^{w}, p_t^{pv} + p_t^{pv,curt} = \bar{p}_t^{pv}, \forall t \quad (17a)$$

$$p_t^{curt} = p_t^{w,curt} + p_t^{pv,curt}, \forall t \quad (17b)$$

$$p_t^{w,curt} \geq 0, p_t^{pv,curt} \geq 0, \forall t \quad (17c)$$

where $\bar{p}_t^w$ and $\bar{p}_t^{pv}$ are the available wind and PV outputs, respectively, while p_t^{curt} is the total renewable curtailment.

(ii) **Unit-level operational feasibility constraints**

Unit-level operational feasibility constraints are represented differently in the two scenarios. In Scenario 1, ANT units may be committed or decommitted as part of the UC/ED scheduling problem. In Scenario 2, each installed ANT unit is assumed to remain online throughout the dispatch horizon, although its output remains subject to the technology-specific operating limits and ramping constraints. This formulation represents a co-generation operating strategy in which short-term balancing is primarily assigned to the co-located electrolyser, thereby reducing the need for repeated reactor shutdown and restart. However, it does not represent or compare alternative commitment strategies involving the temporary shutdown of individual ANT units. The Scenario 2 results should therefore be interpreted as conditional on this imposed operating strategy rather than as a general validation of the optimal commitment strategy for nuclear-hydrogen systems.

Let y_{kit}^{ant} denote the online status of ANT unit i of technology k at time t, and let x_{ki}^{ant} denote its installation status. The turbine electrical output is bounded by:

$$\alpha_{k,\min}^{e}\bar{P}_k y_{kit}^{ant} \le p_{kit}^{tb} \le \bar{P}_k y_{kit}^{ant}, \quad \forall k,i,t \tag{18a}$$

$$y_{kit}^{ant} \le x_{ki}^{ant}, \quad \forall k,i,t \tag{18b}$$

and symmetric hour-to-hour ramp-rate limits restrict inter-temporal changes in turbine output:

$$p_{kit}^{tb} - p_{ki,t-1}^{tb} \le r_k^{ramp}\bar{P}_k, p_{ki,t-1}^{tb} - p_{kit}^{tb} \le r_k^{ramp}\bar{P}_k, \forall k,i,t>1 \tag{19a}$$

$$v_{kit}^{ant} \ge y_{kit}^{ant} - y_{ki,t-1}^{ant}, \quad \forall k,i,t>1 \tag{19b}$$

where v_{kit}^{ant} is the start-up indicator of ANT unit i of technology k at time t.

In Scenario 1, y_{kit}^{ant} is optimised to allow ANT start-up and shut-down decisions. In Scenario 2, the online status of each installed ANT unit is fixed by setting $y_{kit}^{ant} = x_{ki}^{ant}$ for all t. The remaining flexibility is provided through continuous ANT dispatch and the allocation of ANT-derived energy between grid supply and electrolysis.

For low-temperature electrolysis (LTE), the electrical input p_{ut}^{lte} is similarly bounded by installed electrolyser capacity and ramp-limited:

$$0 \le p_{ut}^{lte} \le \bar{P}_{l(u)}^{lte}, \forall u,t \tag{20a}$$

$$p_{ut}^{lte} - p_{u,t-1}^{lte} \le r_{l(u)}^{ramp}\bar{P}_{l(u)}^{lte}, p_{u,t-1}^{lte} - p_{ut}^{lte} \le r_{l(u)}^{ramp}\bar{P}_{l(u)}^{lte}, \forall u,t>1 \tag{20b}$$

where $l(u)$ maps each LTE unit u to its technology type (alkaline or PEM). When high-temperature electrolysis is included, analogous electrical operating limits are imposed on p_{ut}^{soec}.

(iii) **Cross-vector coupling constraints (Scenario 2)**

Cross-vector coupling is activated only when high-temperature electrolysis is enabled. Reactor thermal output q_{kit} is allocated between the steam cycle and electrolysis, consistent with the per-unit heat-balance identity introduced in (1b):

$$q_{kit}^{tb} = q_{kit} - q_{kit}^{el}, \forall k,i,t \tag{21a}$$

Turbine electrical output is then determined as in the ANT model (Eq. (1a)), with the thermal input to the power block given by q_{kit}^{tb}. The diverted heat must meet the SOEC thermal requirement separately for each ANT technology, so that thermal inputs with different heat grades are not pooled:

$$\sum_i q_{kit}^{el} = \sum_{u\in U^{soec}} Q_{kut}^{soec}, \quad \forall k,t \tag{21b}$$

where Q_{kut}^{soec} denotes the thermal input supplied to SOEC unit u from ANT technology k. This technology-specific balance ensures that the SOEC electricity-heat split remains consistent with the outlet temperature T_k of the supplying ANT technology. By contrast, LTE requires no thermal co-input; hence q_{kit}^{el}=0 when only LTE is present.

(iv) **Inherited repurposing constraints**

Repurposing constraints encode legacy site limits that cannot be relaxed in the optimisation. First, the power transfer through the inherited grid connection interface is capped by the available connection capacity:

$$0 \le p_t^{ANT,grid} \le P^{grid}, \quad \forall t \tag{22}$$

where P^{grid} is the inherited grid connection capacity of the retired gas site. This constraint applies only to ANT-derived electricity exported from the repurposed site, $p_t^{ANT,grid}$. External wind and PV generation are system-side inputs and do not pass through the inherited site connection interface.

Second, the total installed footprint of repurposed assets (ANT units plus electrolysers) must not exceed the developed site boundary:

$$\sum_k A_k^{ant} N_k + \sum_r A_l^{el} N_l^{el} \le \bar{A}^{site} \tag{23}$$

where A_k^{ant} and A_r^{el} are the per-unit footprints (e.g., acres/unit) for ANT type k and electrolyser type r, N_k and N_r^{el} are the installed numbers (or capacity-scaled equivalents) selected by the planning decision, and $\bar{A}^{site}$ is the legacy site land limit.

2.3.3. Optimisation methods

The optimisation problems in both configurations are formulated as mixed-integer linear programmes (MILPs), combining discrete planning decisions (technology selection and unit counts) with hourly operational scheduling decisions (unit commitment and dispatch). Simulations are conducted at an hourly resolution over a representative horizon of length Thours. When a reduced horizon is adopted for computational tractability, objective terms expressed on an annual basis are scaled by an annualisation factor to maintain comparability of cost and revenue components.

The MILP formulations are implemented in MATLAB using YALMIP and are solved with Gurobi. To preserve feasibility under extreme operating conditions, slack variables are applied to system-balance constraints and penalised using asymmetric weights, with unserved demand assigned a substantially higher penalty than surplus spillage. Unless stated otherwise, the reported results correspond to the best feasible solution obtained within the prescribed optimality gap and time limit.

2.4. Sensitivity analysis

A sensitivity analysis is applied by perturbing each selected techno-economic input around its baseline using a multiplicative factor, while holding all other assumptions constant, and re-solving the optimisation model to quantify the resulting change in the reported cost metrics. This procedure provides a transparent ranking of influential parameters and clarifies how input uncertainty propagates through the optimisation outcomes. Scenario-specific implementations and results are reported in Sections 4.2.2 (Scenario 1) and 4.3.2 (Scenario 2).

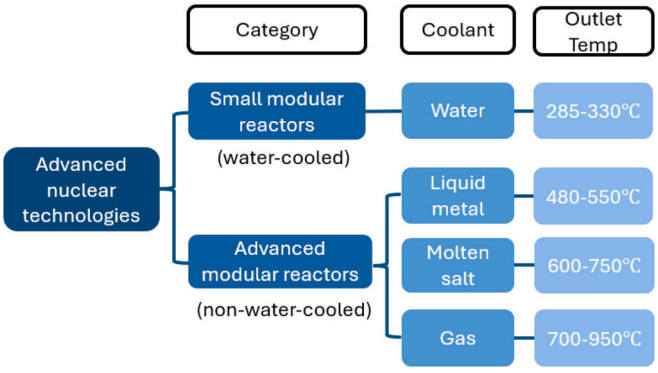


Fig. 4. Classification of Advanced nuclear technologies (ANTs).

3. Techno-economic parameters and assumptions

3.1. ANT techno-economic inputs

As shown in Fig. 4, the UK context typically distinguishes between small modular reactors (SMRs) and advanced modular reactors (AMRs), even though "SMR" is sometimes used internationally as a broader label for modular nuclear concepts [36]. In this study, SMRs are treated as predominantly water-cooled designs, most commonly small pressurised water reactors (PWRs), with moderate outlet temperatures. AMRs, by contrast, are represented as non-water-cooled concepts aligned with Generation IV reactor classes, using alternative primary coolants (e.g., liquid metals, molten salts, or gases) to access higher outlet temperatures. Because outlet temperature determines the usable heat grade, it directly affects the electricity–heat split achievable in high-temperature electrolysis and therefore propagates into hydrogen-production performance and operating economics.

Table 1 summarises the technical and economic parameters adopted for the candidate ANT options considered in the parameter studies, including two water-cooled PWR concepts, advanced high-temperature concepts (HTGR and IMSR), and a microreactor (MR). For each technology, nominal electrical and thermal ratings, an indicative outlet temperature, and key operating parameters are reported to support the UC/ED representation, including minimum stable load, minimum stable turbine load, ramp rate, and minimum downtime. Land-use requirements are represented using reported footprint values and are used to enforce repurposing site-area constraints. Economic inputs are compiled on a consistent basis, including overnight capital cost (USD/kWe), fixed and variable O&M costs, fuel cost, and start-up cost. When multiple modules of the same ANT design are deployed, a within-design learning adjustment is applied to the corresponding CAPEX terms to reflect repeatable delivery and modular deployment effects; the detailed formulation is provided in Appendix A.1.

Because several ANT concepts remain at an early deployment stage, Table 1 distinguishes directly sourced parameters from assumed or proxied inputs through footnotes. Three inputs require particular clarification: minimum downtime, startup fixed cost, and land footprint. The 20 h minimum downtime and 500 USD2020/MWe/startup fixed cost are adopted from Vanatta et al. [9] for a comparable SMR technology set. The downtime assumption is conservative, as reported cooldown times for conventional large reactors to cold shutdown are approximately 10–20 h [37], and the upper end of this range is used here. The startup-cost assumption is also conservative relative to published nuclear planning datasets, which report lower values of approximately 260–278 USD/MWe/start [38]. For footprint values, where the exact design is not available from open sources, a proxy from a closely related reactor variant within the same vendor and reactor family is used. Where the proxy design is larger or more fully specified than the modelled unit, the value is retained directly rather than aggressively downscaled, giving a conservative land-use assumption [12]. These assumptions are therefore intended to avoid overstating either operational flexibility or site deployability. The resulting optimisation outcomes should be interpreted as scenario-specific results under the adopted public-data-based parameterisation, rather than as precise design specifications.

Table 1
Techno-economic and operational assumptions for the candidate ANT options.

Reactor type	PWR470	PWR	HTGR	MSR	Microreactor
Electric power (MWe)	470 [39]	77 [9]	80 [9]	141 [40]	6.7 [9]
Thermal power (MWt)	1358 [12]	250 [9]	200 [41]	300 [40]	20 [9]
Outlet temp (°C)	300 [42]	302 [9]	563 [9]	585 [9]	565 [9]
Minimum stable load (% of REO)	50 [12]	20 [11]	40 [41]	20 [9]	20 [9]
Minimum stable turbine load (% of REO)	10 [9]	10 [9]	10 [9]	10 [9]	10 [9]
Ramp rate (% of REO /h)	240 [12]	40 [9,43]	240 [41]	60 [44]	600 [9]
Minimum downtime (h)[a]	20 [9]	20 [9]	20 [9]	20 [9]	20 [9]
Lifetime (year)	60 [39]	60 [45]	60 [41]	56 [46]	20 [47]
Footprint [acre]	13.47 [12]	2.92 [48]	8.09 [12]	8.7 [12][b]	0.3 [12][b]
Overnight capital cost (10^3 USD/MWe)	5216 [39]	5535 [9]	4569 [9]	4091 [9]	10,902 [9]
Fixed O&M (10^3 USD/MWe-year)	27.4 [39]	115 [9]	100 [9]	85 [9]	264 [9]
Variable O&M (USD/MWhe)	2.33 [39]	0.75 [9]	0 [9][c]	0.5 [9]	0 [9][c]
Fuel cost (USD/MWh)	6.23 [39]	9 [9]	13 [9]	11 [9]	0 [9][d]
Startup fixed cost (USD/Mwe/startup) [a]	500 [9]	500 [9]	500 [9]	500 [9]	500 [9]

[a] Both the minimal down time (20*h*) and the startup fixed cost (500 USD2020/MWe per startup) are assumed values adopted due to the lack of more specific empirical data [9].

[b] Footprint for the exact design was not available from open sources. A proxy value from a closely related reactor variant within the same vendor and reactor family is used for land-use accounting.

[c] Considered 0 due to all O&M allocated to fixed costs [9].

[d] These microreactors have no refuel, and their lifetimes are bound by the initial fuel [9].

Table 2
Techno-economic and operational parameters of electrolyser options.

Electrolyser	SOEC	PEM	ALK
Unit capacity [MW]	50	50	50
Ramp rate [% of unit capacity/h]	30 [49]	100 [49]	50 [49]
Minimum stable load [% of unit capacity/hour]	10 [49]	5 [49]	25 [49]
Standby factor [% of electrical capacity]	8.6 [34]	0 [34]	0 [34]
Stack lifetime [hours]	20,000 [27]	40,000 [27]	80,000 [27]
BOP lifetime [years]	20 [27]	20 [27]	20 [27]
Footprint (including BOP) [m^2/MW]	84 [50]	29.7 [51]	41.5 [52]
Degradation rate [% per 1000 h]	0.59 [35]	0.27 [35]	0.13 [35]
Thermal-integration loss [% of rated capacity]	5 [33]	0 [33]	0 [33]
Stack capital cost [USD /MW]	520,000 [27]	420,000 [27]	340,000 [27]
BOP capital cost [USD/MW]	131,056 [27]	123,556 [27]	123,556 [27]
O&M cost [% of annual CAPEX]	12 [53]	2 [53]	2 [53]

3.2. Electrolyser techno-economic inputs

SOEC is operated at elevated temperature and can utilise both electricity and thermal energy, thereby reducing the electrical input required per unit of hydrogen produced. This feature is exploited in the present framework because ANTs can supply both dispatchable electricity and high-grade heat, allowing the SOEC electricity–heat split to be determined consistently with the selected ANT outlet temperature and operating regime. SOEC is therefore treated as the primary high-temperature pathway, while PEM and ALK are included as electricity-only benchmarks to enable a consistent comparison under identical repurposing constraints and dispatch conditions.

For consistency across the parameter studies, each electrolysis plant is represented as a 50 MW-class unit. Techno-economic inputs and operating assumptions for SOEC, PEM and ALK are summarised in Table 2. Each electrolyser is decomposed into two cost blocks: the electrolysis stack and the balance of plant (BOP). The stack represents the core electrochemical conversion module, while the BOP covers auxiliary subsystems required for stable operation (including power conditioning, feedwater supply and circulation, hydrogen compression and liquefaction where applicable, and thermal management). Performance deterioration is represented for all electrolyser technologies by increasing the electrical specific energy requirement linearly with cumulative represented time, using technology-specific degradation rates from the literature [35]. Land-use requirements are represented through footprint parameters that are applied consistently when enforcing site-area constraints in the optimisation. Similarly, when multiple electrolyser modules of the same technology are deployed, a technology-specific learning adjustment is applied to stack and balance-of-plant CAPEX, while operating-cost terms are kept unchanged; the detailed formulation is provided in Appendix A.1.

3.3. Operating profiles, valuation assumptions and assessment boundary

The present study is formulated as a planning-oriented assessment of brownfield repurposing pathways. Reduced temporal representations are widely adopted in energy-system planning models to balance operational detail against computational tractability. For example, the UK TIMES model represents each of four seasons using a typical day divided into four intra-day periods, resulting in 16 annual time slices [54]. ETI-ESME similarly represents annual demand using diurnal time slices across seasonal conditions [55]. Representative-day structures are also widely used in open-source planning frameworks such as OSeMOSYS [56]. Representative-week formulations are also used or explicitly supported in contemporary capacity-planning tools, including NREL ReEDS and GenX [57,58]. Against this methodological background, the present study adopts four complete historical weeks, one for each meteorological season, with hourly granularity. This retains intra-week chronological variation while maintaining a tractable horizon for the mixed-integer planning-and-scheduling co-optimisation framework.

Historical hourly time-series for Great Britain electricity demand and aggregated wind and solar PV generation were obtained from NESO [59]. Rather than relying on stylised or averaged profiles, complete historical weeks are used to preserve temporal variability and coincidence patterns between demand and variable renewable generation, which are material when evaluating dispatch feasibility and system interactions under repurposing constraints. The year 2024 is selected because it provides the most recent complete and internally consistent dataset.

To construct a compact yet representative set of operating conditions, the 2024 dataset is partitioned into four meteorological seasons. Within each season, all weeks are compared against the seasonal mean profile using mean squared error (MSE) as the distance metric. The comparison is performed on the joint seasonal profiles of demand and renewable generation (equivalently, the implied residual-demand trajectory), ensuring that representative weeks capture the co-variation relevant to dispatch. The week with the minimum MSE is selected for each season, yielding 23–29 April (spring), 16–22 July (summer), 22–28 October (autumn), and 22–28 January (winter). Following seasonal weighting, the aggregated energy volumes estimated from the representative weeks remain within ±5% of the corresponding seasonal values in the original dataset. The selected weeks therefore provide a reasonable representation of seasonal operating conditions for the comparative techno-economic assessment undertaken in this study. Further details on representative-week selection, annualisation, and the limitations of this temporal approximation are provided in Appendix A.2.

For use in site-scale repurposing analysis, the selected weekly profiles are scaled to align with the capacity envelope of the target retired CCGT site. National demand and renewable generation are proportionally scaled to form a site-level net-load trajectory in which wind and PV complement the repurposed plant, while preserving intra-week temporal shapes and coincidence structure. The resulting operating profiles provide an internally consistent basis for optimising repurposing outcomes across configurations.

Price assumptions are specified to support the techno-economic optimisation. A 2024 annual-average wholesale electricity price of £75.7/MWh is adopted based on Ofgem statistics [60], while hydrogen is valued at £9.4/kg-H2 using the official UK HAR1/HAR2 reference, where the £241/MWh-H2 weighted-average strike price is expressed on an HHV basis [61,62]. These values are used as fixed plant-level valuation assumptions rather than forecasts of future market prices. Since the repurposing pathways assessed in this study concern future deployment, and energy prices may rise further under continuing inflationary pressure, policy support mechanisms and supply-chain cost pressures, using 2024 prices provides a conservative basis and helps avoid overstating the economic potential. Future work could further examine the sensitivity of the results to volatile electricity and hydrogen price trajectories and combined parameter uncertainty. These prices are interpreted as plant-gate values and are therefore consistent with a plant-level assessment boundary. Accordingly, the reported LCOE and LCOH quantify the cost of producing electricity and hydrogen within the repurposed site boundary, rather than the delivered cost to final consumers. For electricity, the model represents generation and export through the inherited grid connection, but does not model transmission-network expansion, retail supply costs, balancing-market arrangements, or other downstream electricity-system charges. For hydrogen, the plant boundary includes the electrolyser system, stack replacement, balance-of-plant costs, fixed and variable operating costs, and on-site hydrogen storage and conditioning where represented in the balance of plant. By contrast, downstream hydrogen transport, off-site storage, distribution or delivery infrastructure and end-use conversion are outside the scope of the optimisation. This interpretation is consistent with BEIS [63], which distinguishes production cost from hydrogen delivery, storage, and end-use adaptation costs.

The optimisation is therefore designed to evaluate plant-level repurposing pathways under electricity-balance, operational, site-footprint, and inherited grid-connection constraints. It does not model ANT units or electrolysers as providers of ancillary services, reserve products, or balancing-market services. Planned nuclear refuelling outages and the associated refuelling downtime are also outside the endogenous scheduling scope of the model. These boundary choices are

Table 3
Key characteristics of the Peterhead CCGT repurposing site.

Attribute	Value
Nameplate capacity (MW)	1180
Site footprint (acres)	60.80
Local population density (people per square mile)	19
Coastal location (Yes/No)	Yes
Commissioning year	1982

consistent with the aim of comparing repurposed plant configurations, rather than representing detailed market participation or full nuclear-fuel-cycle operation.

4. Case study and results

4.1. Case description

The case study examined is the Peterhead combined-cycle gas turbine (CCGT) power station in Scotland. The plant was commissioned in 1982 and has an original rated capacity of 1180 MW [64]. Having operated for more than four decades, the site provides a suitable test case for end-of-life transition pathways in which existing energy infrastructure, most notably the grid connection interface and developed industrial land, can be retained and repurposed for low-carbon supply. Screening-relevant site attributes are summarised in Table 3.

Following the screening logic established in Section 2, the Peterhead site satisfies the siting conditions adopted for ANT deployment within the repurposing framework. The surrounding area exhibits a low population density of approximately 19 people per square mile [65], meeting the population-based screening criterion. The coastal location further broadens the candidate technology set under the assumed cooling-availability discriminator, allowing both water-cooled SMR concepts and non-water-cooled AMR concepts to be considered.

In the optimisation, repurposing feasibility is enforced by treating inherited site limits as binding. First, power exchange with the wider grid is capped by the legacy connection envelope (1180 MW), ensuring that any repurposed configuration remains compatible with the existing interface. Second, all new-build assets are constrained by the developed site boundary, represented by an available footprint of 60.80 acres [66]. Under the hydrogen co-generation configuration, residual developable land after accommodating ANT deployment provides the space in which co-located electrolysis may be installed. Within Scenario 2, ANT and electrolyser capacities are jointly optimised subject to the shared site-footprint constraint. For comparative consistency, Scenarios 1 and 2 are evaluated using the same exogenous grid-demand profile, the same available wind and PV generation profiles, and the same inherited grid-export and site-footprint constraints. The scenarios therefore differ in the enabled repurposing configuration rather than in the renewable-energy background or inherited site conditions.

The numerical results obtained for Peterhead should be interpreted as a site-specific demonstration of the proposed repurposing framework rather than as a directly transferable optimum for all retired gas power stations. The framework itself can be re-parameterised for other candidate sites using their inherited grid-export capacity, available industrial land, and renewable operating conditions. Because candidate ANTs are represented as discrete modules with different unit capacities and operational characteristics, variations in connection capacity may lead to different feasible reactor portfolios. Similarly, available land area constrains the combination of ANT and electrolyser units that can be accommodated within the brownfield boundary. Therefore, when applying the proposed framework to other retired gas power stations, sensitivity analysis of key site parameters, such as grid capacity, land availability, and renewable resource conditions, is recommended to support site-specific portfolio screening. In this way, the framework provides a transferable basis for future cross-site assessments while allowing the conclusions to reflect the physical and infrastructural conditions of each candidate site.

Table 4
Summary of technical results for the repurposing case study under Scenario 1.

Metrics	Value
Total installed capacity (MW)	1181.7
Total footprint (acres)	57.3
Annual electricity generation (GWh/yr)	5546.9
Plant-level capacity factor (%)	53.6
Wind curtailment (%)	2.6
PV curtailment (%)	3

4.2. Repurposing with only ANT

4.2.1. Optimal repurposing solution

In Scenario 1 (ANT-only repurposing), the MILP selects a mixed reactor portfolio comprising one PWR470 unit, five molten salt reactor (MSR) units, and one microreactor (MR) unit, giving a total installed capacity of 1181.7 MW. The solution remains consistent with the inherited repurposing constraints. On the network side, the site's grid connection is limited to the original CCGT export capability (1180 MW), which is respected in dispatch. On the land side, the optimal ANT build occupies 57.27 acres, remaining within the available site footprint and preserving the reuse-within-boundary premise.

In aggregate, the optimised ANT portfolio delivers an annual electricity generation of 5546.89 GWh/yr (Table 4), corresponding to a plant-level capacity factor (CF) of 53.58% under the constructed annual profile based on the four representative weeks. This level of utilisation is broadly consistent with the operating regime of the CCGT asset being repurposed, indicating that the optimised ANT configuration can, in aggregate, reproduce the type of duty cycle historically delivered by gas generation at this site, which is an important practical criterion for successful repurposing. However, the resulting capacity factor remains lower than typical nuclear fleet utilisation (e.g., around 72.4% for the UK in 2023), reflecting the fact that the repurposed plant in Scenario 1 is operated within a system context that includes variable wind and PV and does not include any dedicated flexible demand to absorb surplus energy. Consistent with this, modest renewable curtailment is observed, at 2.6% for wind and 3% for PV. In Scenario 1, renewable curtailment arises primarily because the ANT fleet remains subject to minimum stable loading, ramp-rate, and unit-commitment constraints. During certain periods, these constraints require ANT units to maintain a level of electricity output that limits the full utilisation of wind and PV generation. Consequently, a portion of the available renewable output must be curtailed to maintain system-balance feasibility.

Fig. 5 illustrates the economic dispatch of the optimised ANT portfolio through stacked unit-level outputs, revealing a clear division of roles across reactor types. The PWR470 operates at a high utilisation (CF = 86.00%) and provides the effective baseload backbone of the portfolio. This is consistent with its larger unit size and its relatively high minimum stable load requirement (50% of rated output), which naturally favours sustained operation rather than deep turndown. In contrast, the MSR fleet exhibits a much wider feasible operating range because its minimum stable load is lower (20%), enabling more frequent and deeper modulation to follow intra-week variability; correspondingly, its aggregate utilisation is lower (CF = 31.62%), reflecting its role as the principal flexibility provider. Finally, the microreactor, despite its small capacity, shows a high utilisation (CF = 90.94%) and is dispatched to fill residual gaps that remain after the larger units and MSR modulation, thereby improving overall feasibility under the unit-level operating constraints. Taken together, the stacked profile demonstrates how a mixed ANT portfolio can reproduce a CCGT-like duty cycle via intra-fleet load sharing, with flexibility emerging primarily from the MSR operating range and fine balancing supported by the microreactor.

Table 5 shows that the ANT-only repurposing case achieves a plant-level LCOE of 57.90 GBP/MWh under the Scenario 1 operating profile. The one-off grid-connection CAPEX credit is treated as a negative cost in the levelisation, corresponding to an LCOE reduction of 0.125 GBP/MWh. Fig. 6 further indicates that the LCOE is dominated by annualised capital expenditure (CAPEX), which contributes around 60% of total costs, reflecting the high upfront investment characteristic of nuclear technologies. The next largest component is fixed O&M, accounting for approximately 22.1%, followed by fuel cost at 12.9%. This cost structure contrasts sharply with that of a conventional CCGT plant, where fuel

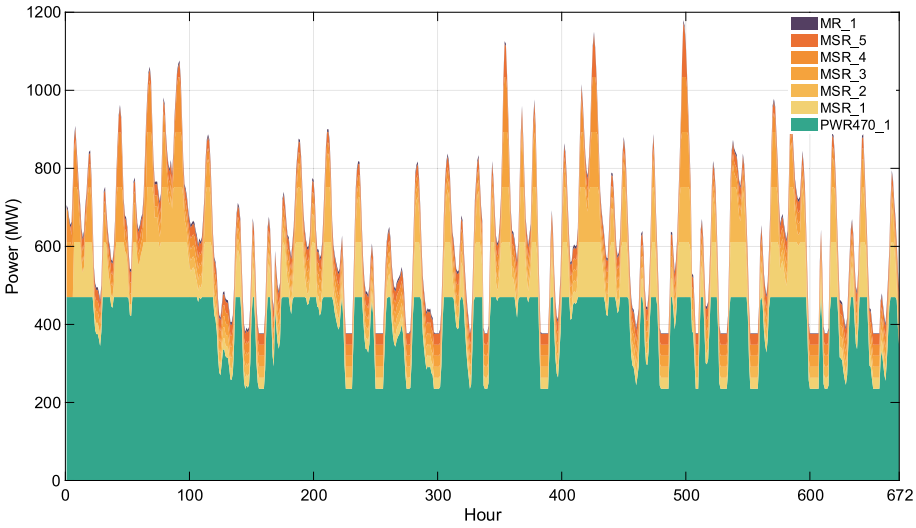


Fig. 5. Plant-level time-varying unit contributions to total electricity output in the ANT-only configuration.

Table 5
Summary of economic results for the repurposing case study under Scenario 1.

Metrics	Value
Plant-level LCOE (GBP/MWh)	57.9
Grid-connection CAPEX credit (one-off, million GBP)	17.3
Discounted payback period (years)	25
IRR (%)	6
NPV (million GBP, $r = 5\%$)	2565.5
Annual net cashflow (million GBP/yr)	291.3

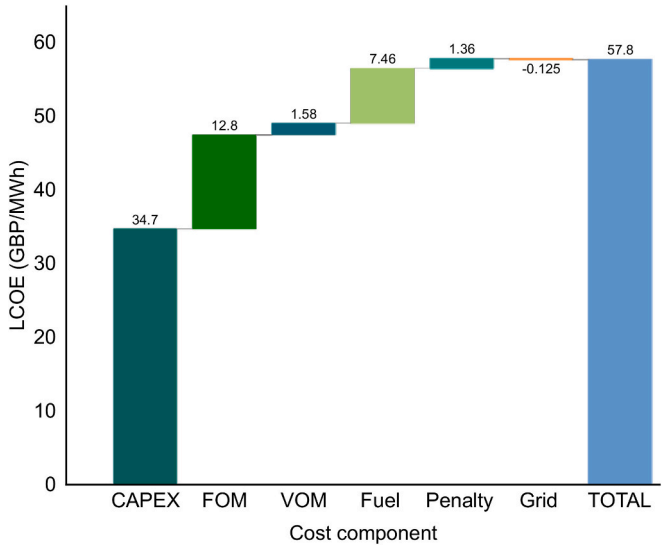


Fig. 6. Plant-level LCOE breakdown for Scenario 1.

expenditure typically constitutes a much larger share of generation cost. In this case, the relatively modest fuel contribution underscores a key economic feature of ANT repurposing, namely, low exposure to variable fuel costs, but also highlights sensitivity to utilisation. The plant-level capacity factor of 53.58% indicates that the high fixed-cost asset is not operated at a typical nuclear baseload level, which increases the levelised cost relative to a higher-capacity-factor nuclear operating regime. Finally, the LCOE decomposition includes a small penalty term (~2.3%), representing the monetised impact of residual curtailment treatment embedded in the optimisation objective.

Beyond LCOE, Table 5 reports the key investment performance indicators. First, the modelled repurposing-related cost saving from reusing existing site assets (notably the grid connection) is treated as an upfront CAPEX credit and is therefore reported both as a one-off saving (17.30 million GBP) and as its equivalent annualised credit when spread across the assumed long-lived asset basis (0.6935 million GBP/yr). The discounted payback period is 25 years, which is materially shorter than the 60-year plant life assumed for nuclear assets; under the adopted price and cost assumptions, the project therefore recovers its discounted investment well within the operating lifetime, leaving a substantial remaining period for value creation beyond capital recovery. The modelled IRR of 6.01% indicates that the project's cashflow profile supports a mid-single-digit project return, which is above the 5% discount rate used in this study and is therefore consistent with a positive investment case under the same assumptions. This is reinforced by a positive NPV (2565.49 million GBP at 5%), implying that the discounted surplus generated over the project life remains positive after accounting for capital and operating costs. The reported annual net cash flow (291.33 million GBP/yr) provides an intuitive measure of operating headroom, reflecting the average annual net surplus generated by the plant under the Scenario 1 dispatch and price assumptions, and helping to contextualise why the payback period and investment indicators remain favourable despite the capital-intensive cost structure.

4.2.2. *LCOE sensitivity to capital-cost uncertainty*

Given the early-deployment status of candidate ANTs, plant-level cost outcomes in Scenario 1 are expected to be most sensitive to uncertainty in upfront investment cost, reflecting FOAK build experience, supply-chain maturity and vendor capacity, licensing and delivery risk, and financing conditions during initial roll-out. To test the robustness of the Scenario 1 repurposing results to this uncertainty, sensitivity is evaluated by varying capital cost assumptions while holding the operating profile and all other techno-economic inputs constant.

As discussed above and evidenced by the LCOE breakdown in Fig. 6, annualised capital expenditure (CAPEX) is the dominant contributor to plant-level LCOE in Scenario 1; the overall cost outcome is therefore most exposed to uncertainty in the underlying upfront investment cost. In this context, the sensitivity analysis is focused on overnight capital cost (OCC), which represents the baseline upfront cost input and directly determines the annualised CAPEX term used in the LCOE calculation. More broadly, ANTs remain an emerging investment proposition and therefore involve substantial cost uncertainty, particularly with respect to FOAK supply chain maturity, regulatory delivery risk, and financing conditions, while large nuclear projects have historically experienced

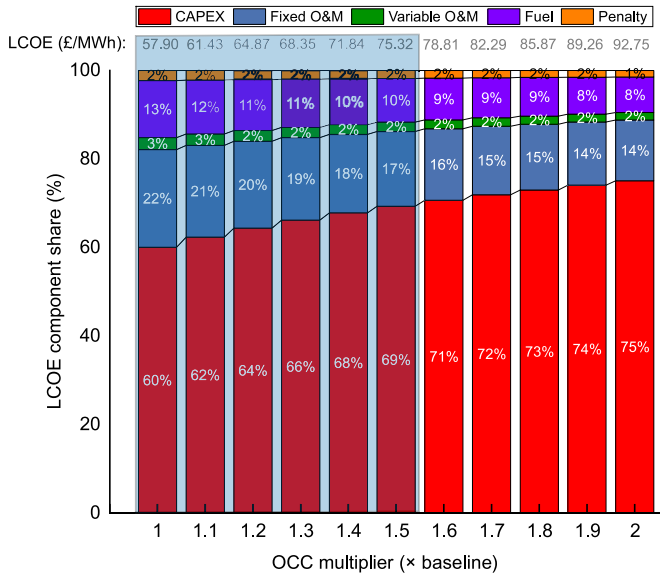


Fig. 7. Decomposition of LCOE into cost components under different OCC multipliers.

cost and schedule overruns that translate into higher effective capital requirements. While ANT-specific modularisation and standardisation are often cited as potential mitigants, capital cost remains the principal near-term uncertainty driver. Accordingly, a one-factor sensitivity analysis is performed by scaling all ANT OCC values by a uniform multiplier from 1.0 to 2.0 (i.e., 100% to 200% of the baseline) in 0.1 increments, holding all other assumptions constant. Fig. 6 reports the resulting plant-level LCOE and its 100% stacked cost decomposition.

Varying the OCC multiplier does not alter the optimal repurposing outcome, and the model selects the same ANT configuration and operating pattern across the full 1.0–2.0 range because OCC is scaled uniformly and therefore does not change the relative techno-economic ordering among candidate reactor options nor the feasibility of the dispatch under Scenario 1 constraints. The impact is instead concentrated in the economic metrics: Fig. 7 shows a near-linear increase in plant-level LCOE from 57.90 GBP/MWh at 1.0× OCC to 92.75 GBP/MWh at 2.0×, with each 10% increase in OCC raising LCOE by approximately 3.49 GBP/MWh on average. Under the assumed electricity price, the repurposing case remains economically viable up to around 1.5× OCC, at which point LCOE reaches 75.32 GBP/MWh, whereas further increases push LCOE above the price benchmark and the investment case is no longer sustained. The 100% stacked decomposition in Fig. 6 further indicates that this sensitivity is driven by the growing dominance of capital costs, with the CAPEX share increasing from around 60% at 1.0× to roughly 75% at 2.0×, while fixed O&M and fuel shares decline in proportional terms because their absolute contributions remain broadly unchanged under the same dispatch and cost assumptions; consequently, delivered capital cost remains the primary lever for maintaining competitiveness in ANT-only repurposing.

Table 6
Summary of technical results for the repurposing case study under Scenario 2.

Metrics	SOEC	PEM	ALK
Optimal ANT portfolio (units)	PWR470 × 3+ MR × 2	PWR470 × 3 + PWR × 4	PWR470 × 3 + PWR × 3
Installed ANT capacity (MW)	1423.4	1718	1641
Electrolyser units (units)	19	23	22
Installed electrolyser capacity (MW)	950	1150	1100
Total footprint (acres)	60.73	60.5	60.5
ANT capacity factor (%)	97.1	96.8	97.3
Electrolyser capacity factor (%)	84.6	90.4	88.4
Wind curtailment (%)	0	0	0
PV curtailment (%)	0	0	0

4.3. Repurposing with nuclear-derived hydrogen co-generation

4.3.1. Optimal co-generation solution

In Scenario 2 (ANT repurposing with co-located SOEC), the MILP selects a PWR470-dominated ANT portfolio supplemented by two microreactors, installing PWR470 × 3 and MR × 2 for a total ANT capacity of 1423.4 MW. This portfolio is paired with 19 SOEC modules, corresponding to 950 MW of electrolysis capacity. On the land side, the ANT units occupy 41.01 acres and the co-located SOEC plant occupies 19.72 acres, giving a total footprint of 60.73 acres within the 60.80-acre site boundary. A summary of the build-out and key indicators is presented in Table 6. Consistency with the inherited repurposing constraints is retained; however, under co-generation the constraint on installed ANT deployment that is implied by the grid-facing interface is substantially relaxed, because a substantial share of nuclear output can be absorbed on-site via hydrogen production rather than being routed through electricity export. On the land side, the combined footprint of the ANTs (41.01 acres) and the co-located SOEC plant (19.72 acres) totals 60.73 acres, remaining within the 60.80-acre site boundary, such that the site footprint is indicated as the primary binding repurposing limit in the optimal build-out. Consequently, nuclear build-out is effectively governed by the availability of an internal demand (SOEC) and the site footprint, rather than by the external export interface alone.

An important limitation of Scenario 2 is that all installed ANT units are required to remain committed throughout the dispatch horizon, with short-term balancing mainly provided by the co-located electrolyser. This imposed commitment strategy restricts the model from selecting temporary or partial unit shutdown when such operation might otherwise be economically preferable. It may therefore increase the simulated nuclear capacity factor and strengthen the apparent LCOE reduction relative to a formulation in which individual ANT units can be shut down and restarted. Accordingly, the reported ANT capacity factor of approximately 97% and the associated LCOE reduction should be interpreted as conditional on the adopted always-online commitment assumption, rather than as generally achievable performance across alternative nuclear operating strategies. Because no partial-shutdown comparison is included, the present analysis cannot quantify the magnitude of this modelling effect.

Separately, the resulting reactor portfolio and electrolyser capacity should therefore be interpreted as a Peterhead-specific optimum under the inherited 1180 MW grid-connection limit and 60.80-acre site boundary, rather than as a universal configuration for retired gas power stations. For application to a specific repurposing project, the optimisation should therefore be re-parameterised using the local grid-connection capacity and available land, and project-specific sensitivity analyses should be conducted to assess the robustness of the resulting configuration.

As a technology comparison within Scenario 2, the co-generation case is also solved using PEM and alkaline (ALK) electrolysers, respectively, while the same inherited repurposing constraints are maintained. Under the PEM configuration, a total of 7 ANT units (3 × PWR470 plus 4 × PWR) is installed, providing 1718 MW of nuclear capacity, and 23 PEM units are installed with an electrolysis capacity of 1150 MW; the combined land requirement is 60.53 acres, which is kept within the 60.80-acre site limit. Under the ALK configuration, 6 ANT units (3 × PWR470 plus 3 × PWR) are installed, delivering 1641 MW, and 22 ALK units are installed totalling 1100 MW of electrolysis capacity, with a similar total land use of 60.45 acres. In both electrolyser options, substantial on-site hydrogen co-production is enabled and higher ANT build-out than under an electricity-export-only regime is supported.

Overall, the optimal build-out is jointly determined by the net-revenue objective and the shared site-footprint constraint. Co-located electrolysis provides an internal outlet for ANT-derived energy, allowing installed ANT capacity to exceed the grid-export limit without implying a sequential allocation of land or capacity.

As summarised in Table 6, coupling ANTs with on-site electrolysis in Scenario 2 is associated with markedly higher ANT utilisation than in Scenario 1: ANT capacity factors of 97.12% (SOEC), 96.84% (PEM) and 97.29% (ALK) are obtained, compared with 53.58% under the ANT-only operating profile. This increase in utilisation is economically material because the ANT levelised cost is dominated by annualised capital expenditure, as previously indicated in Fig. 5, whereas fuel and variable operating costs contribute only a minor share. Accordingly, a higher capacity factor improves capital recovery per unit of output and is therefore expected to reduce the plant-level LCOE relative to a lower-utilisation dispatch regime. This differs from CCGT, where fuel costs typically dominate the overall cost structure. Using the same exogenous renewable energy capacity, Scenario 1 results in wind and PV curtailment rates of 2.6% and 3.0%, respectively (Table 4). By contrast, Scenario 2 eliminates both wind and PV curtailment in all three electrolyser technology cases considered (Table 6). This reduction occurs because the co-located electrolysers provide a flexible local outlet for ANT-derived energy. By locally absorbing ANT-derived electricity and, for SOEC, reactor heat, electrolysis reduces the amount of ANT electricity injected into the wider power system while maintaining feasible ANT operation. This allows a larger share of external wind and PV generation to be accommodated within the system balance, thereby reducing renewable curtailment. These capacity factor and curtailment results are obtained under the selected representative-week simulations and should be interpreted as representative-period outcomes.

These performance gains can be attributed to the introduction of a controllable electrolysis load, through co-located electrolysers, such that plant output is no longer required to be channelled exclusively through the grid-facing electricity pathway. As a result, the need for flexibility to be provided primarily by the ANT fleet itself is materially reduced. In Scenario 1, this requirement is central to the emergence of a more heterogeneous reactor mix that balances economic performance with operational flexibility. This mechanism is further supported by the operating bounds reported in Table 1: the minimum stable load of the reactor island (for example, 50% of rated output for PWR470 and 20–40% for other designs) is typically more restrictive than the minimum stable turbine load (10% of rated output), so under an electricity-only export regime a larger fraction of system variability is forced onto reactor part-load and ramping constraints. Once SOEC is coupled, ANT-derived energy that is not required for grid-facing electricity supply can instead be allocated to hydrogen co-production through turbine electricity and reactor heat, with the thermal contribution expressed in electricity-equivalent terms using the adopted technology-specific heat-to-electricity conversion relationship. Consequently, system balancing is achieved predominantly through time-varying allocation between grid supply and electrolysis demand, rather than through deep modulation of reactor output, thereby reducing the need for flexibility to be embedded in the ANT technology selection.

Reactor outlet temperature affects technology selection indirectly through the SOEC electricity–heat split rather than acting as a standalone selection criterion. Although the MSR offers higher-grade heat and therefore reduces SOEC electrical demand, the objective of Scenario 2 is to maximise the net revenue of the integrated nuclear hydrogen system under the inherited repurposing constraints. Technology selection therefore depends not only on heat grade, but also on discrete reactor module size, available site area, electrical and thermal capacity per unit of constrained land, investment cost, and the ability to satisfy grid-facing electricity demand while supplying the co-located electrolyser. In this case, the incremental efficiency benefit provided by the MSR's higher outlet temperature is outweighed by the portfolio-level advantage of the selected reactor mix, which provides more usable

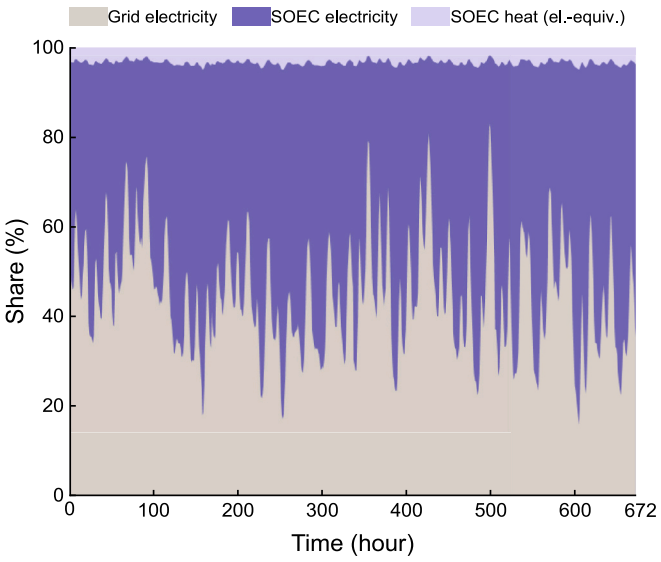


Fig. 8. Plant-level time-varying allocation of ANT-derived energy in the SOEC case, with SOEC heat expressed in electricity-equivalent terms.

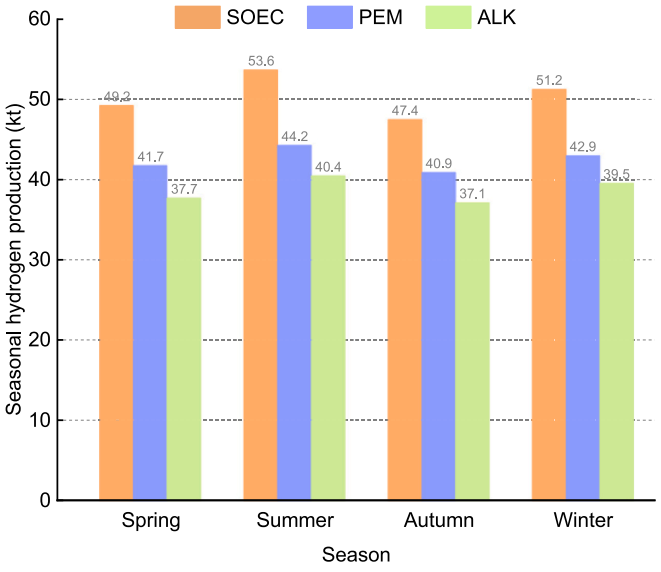


Fig. 9. Seasonal hydrogen production by electrolyser technology.

electrical and thermal capacity within the binding site-footprint constraint. Thus, reactor outlet temperature influences the optimisation through SOEC performance, but the final reactor selection is determined by the overall constrained techno-economic trade-off.

Fig. 8 further illustrates the decomposed plant-level energy allocation into electricity delivered to the grid, electricity supplied to the SOEC, and thermal energy supplied to the SOEC, with heat expressed in electricity-equivalent terms. Across the representative weeks, a substantial share of ANT-derived energy is allocated to electrolysis, while the grid-supplied share varies with system conditions.

Seasonal hydrogen production under Scenario 2 is compared in Fig. 9 for SOEC, PEM and ALK electrolysis, where quarterly values are obtained by scaling the representative-week results using the annualisation factor applied throughout the study. A clear seasonal pattern is observed, with higher hydrogen output in summer and winter than in spring and autumn, which is consistent with the underlying system profiles: during these seasons, the combined effect of higher net system demand and strong renewable availability increases the volume of low-carbon generation that can be diverted into electrolysis demand in the

co-generation configuration, thereby raising the achievable hydrogen throughput. Across all seasons, SOEC is associated with the highest hydrogen production, despite the smallest installed electrolysis capacity and the smallest overall build-out in unit terms, reflecting the benefit of higher conversion efficiency enabled by high-temperature operation and the contribution of co-supplied process heat. By contrast, PEM and ALK exhibit broadly comparable electricity-based energy requirements, with PEM performing marginally better in the optimisation; in addition, the smaller PEM footprint allows more electrolysis capacity (and the associated ANT build-out required to supply it) to be accommodated within the same binding site area, which further explains the higher seasonal hydrogen output achieved under PEM than ALK. Overall, the comparison indicates that SOEC delivers the greatest hydrogen production with the least installed capacity and fewer units, implying a lower upfront capital commitment and reduced investment pressure relative to PEM and ALK, while still capturing the operational benefits of on-site hydrogen co-production.

Enabling on-site electrolysis in the co-generation configuration is expected to improve the overall investment case for ANT repurposing through two reinforcing mechanisms. First, electrolysers provide a controllable local demand sink for ANT-derived energy when grid export is constrained or when dispatch would otherwise reduce nuclear loading. This increases effective utilisation of the repurposed ANT fleet, raising the realised capacity factor and spreading high fixed and annualised capital charges over a larger denominator, which in turn lowers the plant-level LCOE. A lower LCOE benefits both products: electricity can be supplied more competitively, and the electricity component embedded in hydrogen production costs is reduced, improving the implied LCOH for electricity-led pathways and strengthening the value of heat-coupled operation where applicable.

Second, co-generation diversifies and enlarges the revenue stack. In addition to wholesale electricity sales, hydrogen production introduces an additional income stream that can be scheduled flexibly, allowing ANT-derived energy that cannot be exported through the grid-facing pathway to be monetised through hydrogen production. As a result, annual net cash flow is expected to increase relative to power-only repurposing. Taken together, higher utilisation, a lower levelised generation cost, and additional hydrogen revenues are expected to improve the project finance performance of the repurposed ANT investment, reflected in shorter discounted payback periods and higher net present values, while also strengthening the case for electrolyser deployment within the same inherited site constraints. Given this central role of hydrogen co-production in the value stack, the cost composition of hydrogen production is examined next to explain the relative performance of alternative electrolyser options.

Fig. 10 reports the plant-level LCOH decomposition for the hydrogen co-generation configuration across SOEC, PEM and ALK, with a consistent ranking observed: the minimum LCOH is obtained with SOEC coupling, followed by ALK, while PEM yields the highest cost. The ranking is governed primarily by the energy-cost component. For SOEC, the energy-cost share is the lowest (51.2%) because a significant fraction of the process energy requirement is supplied as high-temperature heat rather than electricity; as a result, the specific electricity demand per kilogram of hydrogen is reduced, which constitutes a key mechanism through which the overall energy consumption intensity (and hence energy-driven LCOH) is lowered relative to PEM and ALK. By contrast, energy costs remain dominant for ALK (89.3%) and PEM (81.2%), consistent with largely electricity-led production pathways. A distinct CAPEX–OPEX trade-off is nevertheless indicated for SOEC. The stack CAPEX contribution is the largest (34.9%), exceeding PEM (16.9%) and ALK (8.7%), and is explained in the present parameterisation by the shorter SOEC stack lifetime, which increases the frequency of stack replacement (or the annualised equivalent) and therefore elevates the levelised stack cost contribution. This sensitivity implies clear headroom for cost reduction: as SOEC technology matures and stack lifetime extends towards PEM/ALK levels, a rapid downward shift in the stack CAPEX share and the overall LCOH would be expected, all else equal. In addition, the OPEX share is highest for SOEC (4.4%), consistent with the additional thermal integration and heat/steam-side auxiliaries required in the coupled configuration, whereas PEM (0.4%) and ALK (0.2%) remain near-negligible. Finally, BOP CAPEX contributes only 1.5% to 1.8% across all options, indicating that, under the adopted electrolysis plant cost breakdown, non-stack balance-of-plant components do not primarily explain the LCOH differences between technologies in Scenario 2. Overall, the results indicate that the reduction in electricity intensity enabled by ANT–SOEC heat coupling more than offsets the higher stack-related cost and elevated operating complexity, leading to the lowest plant-level LCOH among the candidate electrolysis technologies under Scenario 2 assumptions.

4.3.2. *LCOH sensitivity under electrolyser coupling*

Given the early-deployment status of candidate ANTs and the degradation- and replacement-sensitive components introduced by electrolysis, uncertainty remains in several techno-economic inputs and can propagate into the LCOH outcomes reported for Scenario 2. A structured one-at-a-time sensitivity analysis is therefore conducted by perturbing each selected parameter around its baseline using a multiplicative factor while holding all other assumptions constant, with the

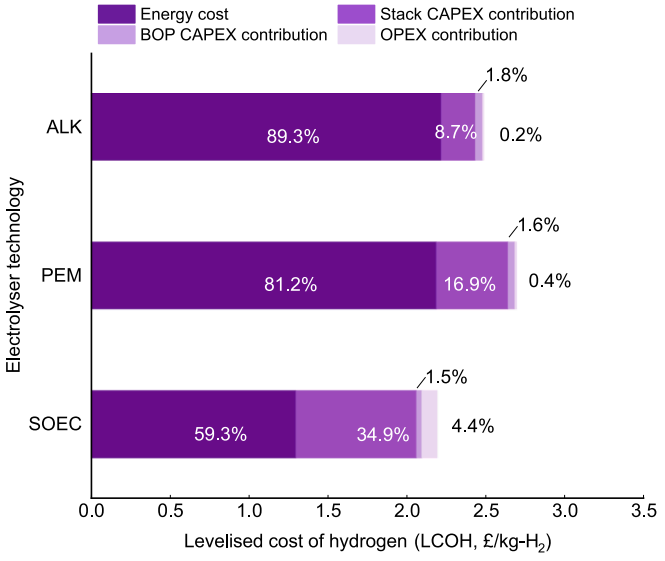


Fig. 10. Plant-level LCOH breakdown under Scenario 2 for three electrolyser technologies.

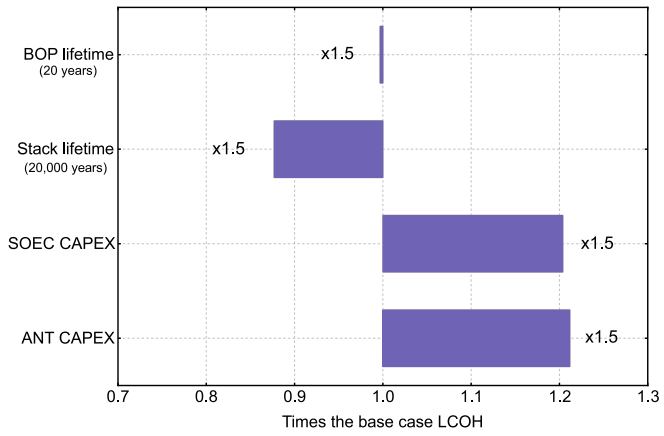


Fig. 11. Normalised sensitivity of LCOH to key ANT and SOEC techno-economic parameters in Scenario 2.

optimisation model re-solved to quantify the corresponding LCOH response. For Scenario 2, the sensitivity set spans both nuclear-side and electrolysis-side drivers, with multipliers applied to ANT CAPEX and electrolyser CAPEX, and lifetime uncertainty represented through stack lifetime and balance-of-plant lifetime. The Scenario 2 sensitivity results are evaluated primarily against plant-level LCOH, and are reported in normalised form to provide a transparent ranking of influential cost and lifetime drivers for the co-located hydrogen-production configuration.

Fig. 11 presents the normalised LCOH response of the Scenario 2 SOEC case to a 50% (1.5×) increase in selected nuclear- and electrolysis-side parameters. The largest upward driver is ANT CAPEX: a 50% increase raises LCOH by 21.2%. SOEC CAPEX is nearly as influential, increasing LCOH by 20.4%. By contrast, lifetime-related parameters act through the annualised replacement burden. Increasing stack lifetime by 50% reduces LCOH by 12.3%, reflecting the strong sensitivity of SOEC economics to stack durability and replacement frequency. This response is consistent with the cost structure observed in Fig. 10, where stack-related costs account for a large share of SOEC LCOH: improvements in durability reduce the annualised stack replacement cost and translate directly into a lower levelised hydrogen cost. The implication is that, as SOEC technology matures and stack lifetime extends towards PEM/ALK levels, a rapid reduction in LCOH would be expected. In contrast, increasing balance-of-plant lifetime by 50% reduces LCOH by only 0.3%, indicating that uncertainty in non-stack component longevity has a negligible influence on LCOH in the present configuration. Overall, Fig. 11 identifies ANT CAPEX and SOEC CAPEX as the principal upward sensitivity drivers, while stack lifetime remains the main durability-related lever.

5. Conclusion

This study formulates a repurposing-oriented optimisation framework to identify least-cost, practically feasible pathways for converting an end-of-life gas power station into a modular nuclear plant and extending to accommodate hydrogen co-generation. In doing so, the model enforces inherited brownfield constraints, particularly the legacy grid connection limit and available land footprint, so that technology selection and operation are assessed subject to realistic site constraints. It also represents HTSE coupling in a thermodynamically consistent way by linking the SOEC electricity–heat split to reactor heat grade, which is governed by the chosen ANT technology and its outlet temperature, and it lightly accounts for modular deployment effects through learning-based cost reductions when multiple reactor modules are installed.

The results first show that the selected ANT portfolio can provide flexibility comparable to the CCGT benchmark, allowing the repurposed plant to support demand following rather than operating only as base-load generation. Nuclear-hydrogen integration further strengthens this flexibility. The co-located electrolyser provides a flexible local demand that can absorb ANT-derived electricity and, for SOEC, reactor heat when these outputs are not required for grid-facing supply. This additional outlet reduces the amount of ANT electricity that must be exported due to operational constraints, while preserving the ability to meet grid demand. As a result, renewable curtailment is eliminated in the nuclear-hydrogen integration cases, and the repurposed plant can accommodate more variable system conditions through coordinated allocation between grid supply and hydrogen production. For the Peterhead case study, and based on the adopted techno-economic assumptions alongside representative-week simulations, SOEC coupling provides the strongest hydrogen co-generation pathway among the electrolyser options considered. By providing a flexible local outlet for nuclear-derived electricity and heat, nuclear-hydrogen integration substantially increases reactor utilisation, reducing the plant-level LCOE by about 32% relative to power-only repurposing. The SOEC pathway also gives the lowest plant-level LCOH, at about 2.2 GBP/kg-H2, while requiring the lowest upfront investment and producing the largest hydrogen output. This reflects its higher conversion efficiency, because high-temperature electrolysis can use both electricity and cost-effective nuclear heat. Sensitivity analysis indicates that LCOH remains most exposed to capital-cost assumptions: a 50% increase in ANT CAPEX and SOEC CAPEX raises LCOH by 21.2% and 20.4%, respectively, while a 50% increase in stack lifetime reduces LCOH by 12.3%. Because electricity and hydrogen prices are treated as fixed plant-level valuation assumptions in this study, the reported economic advantage should be interpreted as a site-specific result under the adopted price assumptions, rather than as a robustness proof under future electricity- and hydrogen-market price uncertainty. These findings indicate that, for the Peterhead case and under the adopted techno-economic assumptions, nuclear-hydrogen integration, particularly through SOEC coupling, can improve the techno-economic value of brownfield nuclear repurposing where both grid-export and site-footprint constraints are material.

The Scenario 2 results are conditional on the assumption that all installed ANT units remain online, with short-term balancing mainly provided by the co-located electrolyser. This assumption may favour high nuclear utilisation and strengthen the estimated LCOE benefit of hydrogen co-generation. In addition, the selected representative-week simulations do not constitute a full-year chronological validation. Future work will therefore examine alternative unit-commitment strategies that allow partial reactor shutdown and restart and extend the baseline SOEC case to an 8760-h simulation, thereby assessing the robustness of the reported capacity factor, renewable-curtailment outcome, LCOE and LCOH under a wider range of operating conditions.Overall, the study highlights the value of treating retired gas power stations not simply as decommissioned assets, but as constrained brownfield platforms where modular nuclear power and hydrogen co-generation can be jointly optimised. As advanced nuclear technologies emerge, conventional thermal power stations retire, and electrolyser technologies continue to mature, the proposed framework can provide a useful methodology for assessing other brownfield repurposing opportunities. However, the framework is transferable only as an assessment methodology, rather than as a universal portfolio prescription. For any specific project, the model must be re-parameterised using the local grid-connection capacity, available land, market conditions and technology assumptions, and project-specific sensitivity analyses should be undertaken to evaluate the robustness of the resulting configuration.

CRediT authorship contribution statement

Ruiyang He: Writing – original draft, Visualization, Software, Data curation, Conceptualization. **Jianzhong Wu:** Writing – review & editing, Investigation, Funding acquisition, Conceptualization. **Shuai Yao:** Project administration, Methodology.

Declaration of competing interest

The authors declare that they have no known competing financial interests or personal relationships that could have appeared to influence the work reported in this paper.

Acknowledgement

This work was supported by the EPSRC “Hydrogen Integration for Accelerated Energy Transitions Hub (HI-ACT)” project (EP/X038823/2), EPSRC “Supergen Energy Networks Impact Hub” project (EP/Y016114/2) and UK Energy Research Centre Phase 5 (grant number UKRI098).

Appendix A. Appendix

A.1. Learning-curve formulation for ANTs and electrolysers

A learning-curve adjustment is included to represent cost reductions from repeatable deployment of modular technologies. The learning formulation follows the National Nuclear Laboratory [18], where the cost reduction observed for successive South Korean nuclear builds, originally reported by Lovering et al. [67], was used to estimate a learning rate of 11.76%. Ref. [18] further applied the same learning formulation to the hydrogen generation plant and explicitly evaluated the effect of learning on plant CAPEX.

In this study, the same learning curve is applied and the cost of the Nth unit of a given technology is modelled as:

$$C_N = C_1 N^{log_2(1-LR)} \tag{A1}$$

where C_N is the CAPEX of the Nth unit, C_1 is the first-of-a-kind CAPEX, N is the within-technology deployment order, and LR = 11.76% is the learning rate.

The learning adjustment is applied separately within each technology type and does not transfer across different reactor or electrolyser designs. For ANTs, learning is applied to the overnight capital cost of repeated modules of the same reactor design. For electrolysis technologies, learning is applied to electrolyser capital cost, including stack and balance-of-plant CAPEX, when multiple modules of the same electrolyser technology are deployed.

It should be noted that the learning factor is applied only to CAPEX, as the learning-curve formulation primarily represents cost reductions achieved through successive technology deployment. OPEX learning effects are not included because reliable empirical evidence for such effects remains limited for ANTs and electrolysers, and OPEX represents a relatively smaller cost component in the present analysis. If robust data become available, OPEX learning effects could be incorporated in future work.

A.2. Representative-week selection and annualisation

The present study adopts four seasonal representative weeks to retain hourly operational detail while maintaining a tractable computational horizon for the mixed-integer planning-and-scheduling framework. The hourly dataset is partitioned into four meteorological seasons: spring (March–May), summer (June–August), autumn (September–November), and winter (December–February). A complete historical week is selected for each season based on its ability to represent the corresponding seasonal electricity-demand profile. The selected weeks are shown in Table A.2.

Table A.2
Selected representative weeks and seasonal electricity-demand deviations.

Season	Selected historical week	Deviation from seasonal demand volume
Spring	23–29 April 2024	+4.11%
Summer	16–22 July 2024	+3.332%
Autumn	22–28 October 2024	−1.36%
Winter	22–28 January 2024	−2.55%

For annualisation, the hourly results obtained for each representative week are weighted according to the duration of the corresponding meteorological season. For an hourly operating quantity x, the annualised value is calculated as:

$$X_{\text{annual}} = \sum_{s \in S} \frac{D_s}{7} \sum_{t=1}^{168} x_{s,t} \tag{A2}$$

where S denotes the four seasons, D_s is the number of days in season s, and $x_{s,t}$ is the hourly value in representative week s. This weighting procedure is applied to energy output, renewable curtailment, hydrogen production, variable operating costs, and revenues. Following seasonal weighting, the aggregated electricity-demand volumes estimated from the representative weeks remain within ±5% of the corresponding seasonal values in the original dataset. The annual weighted deviation is approximately +0.62%. The selected historical weeks therefore provide a consistent representation of seasonal demand conditions while retaining hourly sequencing, weekday-weekend variation, and the observed intra-week coincidence between demand and variable renewable generation. Compared with discrete time slices or representative-day structures commonly adopted in planning models, this approach offers a richer chronological representation without imposing the computational burden of a full-year mixed-integer optimisation.

A full 8760-h chronological simulation would provide a complementary level of operational resolution, particularly for project-specific assessments in which infrequent demand peaks, prolonged periods of unusually high or low renewable generation, or sustained price variations are of interest. Capturing these conditions in greater detail may refine the absolute estimates of renewable curtailment, ANT and electrolyser capacity factors, hydrogen output, LCOE, and LCOH. However, the representative-week approach is appropriate for the purpose of the present study, which is to compare brownfield repurposing pathways on a consistent basis and identify their principal techno-economic characteristics. Full-year chronological validation would be a valuable subsequent step when applying the framework to detailed project design or capacity-adequacy assessment.

Data availability

Data will be made available on request.

References

[1] https://www.gov.uk/government/publications/clean-energy-superpower-mission-areas-of-research-interest/clean-energy-superpower-mission-areas-of-research-interest n.d.

[2] https://www.neso.energy/publications/future-energy-scenarios-fes/fes-documents n.d.
[3] https://www.gov.uk/government/publications/electricity-generation-costs-2023 n.d.
[4] Systems CE. Electricity networks commissioner –companion report findings and recommendations. 2023.
[5] Rogers P. Midlands nuclear siting study: main report. Equilibrion; 2025.
[6] https://decarbonization.visualcapitalist.com/visualized-the-four-benefits-of-small-modular-reactors/ n.d.
[7] He R, Yang H, Sun S, Lu L, Sun H, Gao X. A machine learning-based fatigue loads and power prediction method for wind turbines under yaw control. Appl Energy 2022;326:120013.
[8] Lu H, Gao X, Yu J, Zhao Q, Zhu X, Ma W, et al. Analysis and prediction of incoming wind speed for turbines in complex wind farm : accounting for meteorological factors and spatiotemporal characteristics of wind farm. Appl Energy 2025;381:125135. https://doi.org/10.1016/j.apenergy.2024.125135.
[9] Vanatta M, Patel D, Allen T, Cooper D, Craig MT. Technoeconomic analysis of small modular reactors decarbonizing industrial process heat. Joule 2023;7:713–37. https://doi.org/10.1016/j.joule.2023.03.009.
[10] Jenkins JD, Zhou Z, Ponciroli R, Vilim RB, Ganda F, de Sisternes F, et al. The benefits of nuclear flexibility in power system operations with renewable energy. Appl Energy 2018;222:872–84. https://doi.org/10.1016/j.apenergy.2018.03.002.
[11] Evaluation methodology for the stability of the NuScale power module. 2020.
[12] Elbokl T. Small modular reactors catalogue 2024. IAEA; 2024. p. 24–7. https://doi.org/10.61092/iaea.3o4h-svum. 143.
[13] https://www.gov.uk/government/news/rolls-royce-smr-selected-to-build-small-modular-nuclear-reactors n.d.
[14] Xu Z, Gao X, Ma H, Zhong Z, Han Z. Dynamic coupling of wake added turbulence and array effects : nonlinear impacts on power performance and fatigue damage of 22 MW floating offshore wind turbines. Renew Energy 2026;263:125441. https://doi.org/10.1016/j.renene.2026.125441.
[15] Lin W. Optimised scheduling of integrated energy system refined hydrogen utilisation. 2025. https://doi.org/10.1049/esi2.70018.
[16] Xiao H, Liu Z, Pei W, Beshir M. Multi-scale coordinated optimal dispatch method of electricity-thermal-hydrogen integrated energy systems. IET Energy Syst Integr 2023:275–89. https://doi.org/10.1049/esi2.12100.
[17] Integrated co-optimisation of energy–water–hydrogen systems for carbon-aware dispatch under uncertainty. 2026. p. 1–14. https://doi.org/10.1049/esi2.70053.
[18] Connolly C, Taylor K, Bankhead M, Jarvis R, Dean J. Techno-economic analysis of heat-assisted hydrogen production from nuclear power. New Energy Exploit Appl 2024;3:108–29. https://doi.org/10.54963/neea.v3i1.234.
[19] Matthews J. The road to net zero : renewables and nuclear working together. 2024. :1–79.
[20] Nie X, Cheng M, Zuo X, Dai Z. Techno-economic assessment of a smTMSR-based nuclear–renewable hybrid energy system with high-temperature steam electrolysis. Nucl Eng Des 2025;440:114138. https://doi.org/10.1016/j.nucengdes.2025.114138.
[21] Kim JS, Boardman RD, Bragg-Sitton SM. Dynamic performance analysis of a high-temperature steam electrolysis plant integrated within nuclear-renewable hybrid energy systems. Appl Energy 2018;228:2090–110. https://doi.org/10.1016/j.apenergy.2018.07.060.
[22] Rahman J, Jacob RA, Zhang J. Multi-timescale power system operations for electrolytic hydrogen generation in integrated nuclear-renewable energy systems. Appl Energy 2025;377:124346. https://doi.org/10.1016/j.apenergy.2024.124346.
[23] Frick K, Wendt D, Talbot P, Rabiti C, Boardman R. Technoeconomic assessment of hydrogen cogeneration via high temperature steam electrolysis with a light-water reactor. Appl Energy 2022;306:118044. https://doi.org/10.1016/j.apenergy.2021.118044.
[24] Locatelli G, Boarin S, Fiordaliso A, Ricotti ME. Load following of small modular reactors (SMR) by cogeneration of hydrogen: a techno-economic analysis. Energy 2018;148:494–505. https://doi.org/10.1016/j.energy.2018.01.041.
[25] Slavin B, Wang R, Roy D, Ling-Chin J, Roskilly AP. Techno-economic analysis of direct air carbon capture and hydrogen production integrated with a small modular reactor. Appl Energy 2024;356:122407. https://doi.org/10.1016/j.apenergy.2023.122407.
[26] Temiz M, Dincer I. Development of a hybridized small modular reactor and solar-based energy system for useful commodities required for sustainable cities. Energy 2024;286:129562. https://doi.org/10.1016/j.energy.2023.129562.
[27] Jang D, Kim J, Kim D, Han WB, Kang S. Techno-economic analysis and Monte Carlo simulation of green hydrogen production technology through various water electrolysis technologies. Energy Convers Manag 2022;258:115499. https://doi.org/10.1016/j.enconman.2022.115499.
[28] Bui T, Lee D, Ahn KY, Kim YS. Techno-economic analysis of high-power solid oxide electrolysis cell system. Energy Convers Manag 2023;278. https://doi.org/10.1016/j.enconman.2023.116704.
[29] Min J, Lee S, Hoon D, Jae H, Park W, Shin J, et al. Environ-economic analysis of high-temperature steam electrolysis for decentralized hydrogen production. Energy Convers Manag 2022;266:115856. https://doi.org/10.1016/j.enconman.2022.115856.
[30] Hill D, Martin A, Martin-Nelson N, Granger C, Memmott M, Powell K, et al. Techno-economic sensitivity analysis for combined design and operation of a small modular reactor hybrid energy system. Int J Thermofluids 2022;16:100191. https://doi.org/10.1016/j.ijft.2022.100191.
[31] Sadeghi K, Ghazaie SH, Sokolova E, Sergeev V, Ksenia N, Yang L. Machine learning-based correlation for economic evaluation of HTSE-nuclear cogeneration plant. Int J Hydrog Energy 2025;114:337–51. https://doi.org/10.1016/j.ijhydene.2025.02.423.
[32] Zhang T. Techno-economic analysis of a nuclear-wind hybrid system with hydrogen storage. J Energy Storage 2022;46:103807. https://doi.org/10.1016/j.est.2021.103807.
[33] Data T, High FOR, Solid T, Electrolyser O, Electrolysers a. Technology data for high temperature solid oxide electrolyser cells , alkali and pem electrolysers n.d.:1–16.
[34] Roeder T, Rosenstiel A, Monnerie N, Sattler C. Impact of expected cost reduction and lifetime extension of electrolysis stacks on hydrogen production costs. Int J Hydrog Energy 2024;95:1242–51. https://doi.org/10.1016/j.ijhydene.2024.08.015.
[35] Guan D, Wang B, Zhang J, Shi DR, Jiao DK, Li L. Hydrogen society: from present to future. 2023.
[36] https://www.gov.uk/government/publications/advanced-nuclear-technologies/advanced-nuclear-technologies n.d.
[37] https://www.nuclear-power.com/nuclear-power/reactor-physics/reactor-operation/reactor-cooling/ n.d.
[38] Jagt S Van Der, Patankar N, Jenkins JD. Understanding the role and design space of demand sinks in low-carbon power systems. Energy Clim Chang 2024;5:100132. https://doi.org/10.1016/j.egycc.2024.100132.
[39] Steigerwald B, Weibezahn J, Slowik M, von Hirschhausen C. Uncertainties in estimating production costs of future nuclear technologies: a model-based analysis of small modular reactors. Energy 2023;281:128204. https://doi.org/10.1016/j.energy.2023.128204.
[40] Samalova L, Chvala O, Maldonado GI. Comparative economic analysis of the integral molten salt reactor and an advanced PWR using the G4-ECONS methodology. Ann Nucl Energy 2017;99:258–65. https://doi.org/10.1016/j.anucene.2016.09.001.
[41] Crowell J. X-energy: XE-100 reactor the key to an integrated energy system, reliable baseload, agile load following, industrial applications. 2019.
[42] https://gda.rolls-royce-smr.com/our-technology n.d.
[43] Alhadhrami S, Soto GJ, Lindley B. Economic dispatch optimization of multi-unit SMR site. Trans Am Nucl Soc 2022;127:879–82. https://doi.org/10.13182/T127-39610.
[44] Singh V, Lish MR, Chvála O, Upadhyaya BR. Dynamics and control of molten-salt breeder reactor. Nucl Eng Technol 2017;49:887–95. https://doi.org/10.1016/j.net.2017.06.003.
[45] Power N. NuScale small modular reactor integration for hydrogen and ammonia production. 2025.
[46] https://en.wikipedia.org/wiki/Integral_Molten_Salt_Reactor n.d.
[47] https://www.usnc.com/mmr/ n.d.
[48] https://inl.gov/trending-topics/small-modular-reactors n.d.
[49] Gu Z, Pan G, Gu W, Zhou S, Wu Z, Lu S. Assessment and prospect of region joint electrolytic hydrogen systems considering multiple energy sources: wind, solar, hydro and thermal power. IEEE Trans Ind Appl 2023;59:5269–82. https://doi.org/10.1109/TIA.2023.3282923.
[50] SOEC High-temperature electrolysis. 2026. n.d.
[51] https://www.ohmium.com/news/ohmiums-comprehensive-and-modular-hydrogen-solution-achieves-a-compact-horizontal-footprint-of-29-7-m2-mw-including-maintenance-and-access-areas n.d.
[52] Customer R, Excellence S, Every A, Of S, Electrolyzer T, Cycle L. Sunfire-hylink alkaline. 2025. p. 7–8.
[53] Berrada A, Sanjari MJ, El Mrabet R. Techno-economic assessment of hydrogen production: comparative analysis of electrolyser technologies in a hybrid PV/wind system. Int J Hydrog Energy 2025;141:193–211. https://doi.org/10.1016/j.ijhydene.2025.05.384.
[54] Daly HE, Fais B. UK times model overview. 2014.
[55] Wills J, Heaton C, Milne S, Middleton M, Milne S, Milne S, et al. DECC small modular reactor techno-economic assessment – project 2 technical report. 2016.
[56] https://osemosys-global.readthedocs.io/en/latest/getting-started.html n.d.
[57] https://github.com/NatLabRockies/ReEDS-2.0 n.d.
[58] https://genxproject.github.io/GenX.jl/v0.3.6/data_documentation.html n.d.
[59] https://www.neso.energy/data-portal n.d.
[60] https://www.ofgem.gov.uk/news-and-insight/data/data-portal/wholesale-market-indicators n.d.
[61] https://www.gov.uk/government/publications/hydrogen-production-business-model-net-zero-hydrogen-fund-shortlisted-projects/hydrogen-production-business-model-net-zero-hydrogen-fund-har1-successful-projects n.d.
[62] https://www.gov.uk/government/publications/hydrogen-allocation-round-2/har2-clarification-questions n.d.
[63] https://www.gov.uk/government/publications/hydrogen-production-costs-2021 n.d.
[64] https://www.ssethermal.com/flexible-generation/operational/peterhead/ n.d.
[65] https://www.ons.gov.uk/explore-local-statistics/indicators/population-density n.d.
[66] https://openinframap.org n.d.
[67] Lovering JR, Yip A, Nordhaus T. Historical construction costs of global nuclear power reactors. Energy Policy 2016;91:371–82. https://doi.org/10.1016/j.enpol.2016.01.011.